



## Master Thesis



# “Along strike variation of active fault arrays and their effect on landscape morphology in the northwestern Himalaya”

Author:

Markus Nennewitz

Mat-Nr.: 754570

1. Examiner: Dr. Rasmus C. Thiede

2. Examiner: Prof. Dr. Bodo Bookhagen

---

## **Declaration of plagiarism**

I hereby declare that this thesis is the result of my own independent work, and that in all cases material from the work of others (in books, articles, essays, dissertations, and on the internet) is acknowledged, and quotations and paraphrases are clearly indicated. No other material than that listed has been used.

## Acknowledgements

First of all I would like to thank my supervisors Dr. Rasmus Thiede and Prof. Dr. Bodo Bookhagen, who broadend my mind for active tectonics and geomorphology during many meetings and even more e-mail conversations. They supported me in every minute of my work and were always open for questions from my side. Furthermore, I thank them and the DAAD for giving me the opportunity to go on a field trip in NW India. According to that, I would like to mention that I really appreciated the stay at the IIT Gandhinagar for which I also thank Prof. Dr. Vikrant Jain and his Phd-students. Furthermore, I have to thank Saptarshi Dey and Patricia Eugster for providing data files necessary for my analysis. And last but definitely not least I thank my girlfriend and my parents for their tremendous amount of support and for being patient with me during my ongoing work.

## Abstract

The location and magnitude of the active deformation of the Himalaya has been in the interest for many decades. Still the understanding of the neotectonics and its effect on the regional topography is improvable. This study investigates the along strike changes of fault activity and segmentation in the northwestern Himalaya. Therefore we have performed a river network analysis and obtained the channel steepness indexes for tributaries with a drainage area falling in a range of  $1\text{km}^2$  to  $100\text{km}^2$ . The indexes were averaged over catchments with a Strahler-order of 3. We used orogen-perpendicular and along strike profiles to determine areas of equal subsurface geometries and active fault segments within. The observed pattern of along strike variation in fault activity leads to the conclusion that three segments (A1-A3) operate independently from each other. A1 covers the Dehra Dun, the Nahan Salient and the Garwhal region. A2 is located in the Kangra Dun and the Chamba Himalaya. A3 contains the Kashmir Himalaya and the respective foreland fold- and thrust-belt. Despite the differences in the structural architecture of the orogenic front, we found good reason for an out-of-sequence activity of segments of the PT2 promoting structure, as well as of fault segments of the MBT in all three areas since the Pleistocene.

## Zusammenfassung

Das Verständniss von neotektonischen Prozessen im Nordwest Himalaya wurde bereits in vielen Studien untersucht. Dennoch haben wir Grund zur Annahme, dass dieses Verständniss ausbaufähig ist. Speziell die Aktivität von einzelnen Störungssegmenten entlang der MBT und der geologischen Struktur unterhalb der PT2 wurde noch nicht weitreichend analysiert. Wir haben die  $k_{sn}$ -Werte einzelner Segmente von Zuflüssen mit einer Einzugsgebiet von  $1\text{km}^2$  bis zu  $100\text{km}^2$  im Untersuchungsgebiet ermittelt. Wir haben die Werte für einzelne Wassereinzugsgebiete gemittelt und mithilfe von orthogonalen Profilen und Profilen, die parallel zum Streichen von Störungen verlaufen, analysiert und in den Zusammenhang gebracht. Durch diese Methode können wir Aussagen über die regionale Varianz in den Erosionsraten treffen, welche uns unter bestimmten Voraussetzungen wiederum auch auf Unterschiede in der tektonischen Aktivität von Störungen schließen lässt. Im Zuge der Untersuchung stellte sich heraus, das es drei Gebiete im nordwest Himalaya gibt, die nur durch einen unterschiedlichen strukturgeologischen Aufbau zu erklären sind (A1-A3). Trotz dieses Unterschiedes fanden wir heraus, dass es im gesamten Untersuchungsgebiet entlang der Front des Hohen Himalaya und entlang der MBT eine out-of-sequence Aktivität von einzelnen Störungssegmenten gibt.

## Table of Contents

Abstract .....	3
Introduction.....	6
Geologic setting.....	8
Tectonic evolution and recent setting.....	8
Description of physiographic units .....	11
Theories for the accommodation of the crustal shortening .....	12
Direction and velocity of plate motion.....	13
Seismic activity and geodetic velocities in NW India.....	14
Methods .....	16
River steepness and concavity index.....	16
Knickpoints in longitudinal river profiles.....	18
Processing the channel steepness indexes .....	19
Post-processing steepness indexes .....	21
Correction for glacial erosion .....	21
Catchment-wide steepness index .....	21
Hot Spot Analysis.....	22
Topometric analysis.....	22
Orthogonal swath profiles.....	22
Parallel swath profiles .....	23
Results .....	25
Channel steepness in the NW Himalaya.....	25
Description of the perpendicular swath profiles.....	26
Summary of profile 1-10.....	32
The cumulative height.....	33
Description of fault-parallel swath profiles.....	34
Discussion .....	37
Significance in data distribution .....	37
Applicability of the method .....	38
Active out-of-sequence thrusting vs. elastic behavior of the upper plate.....	40
Area A1 - A Central Himalayan analogue .....	41
Area A2 – The Chamba Himalaya .....	43
Area A3 – The Kashmir Himalaya .....	44
Along strike variations .....	46
Recent denudation at the PT2.....	46

Tectonic activity of MBT-Segments .....	47
Total strain distribution .....	49
Relationship to published rates.....	50
Relation to exhumation and denudation rates .....	52
Conclusion .....	55
Reference.....	56

## Introduction

The continental collision of India and Eurasia has formed the highest recent orogen on earth, the Himalaya. The ongoing north-north-east oriented motion of the Indian plate still leads to active tectonics. Major thrust systems bounding the physiographic units of the Himalaya and the Tibetan plateau accommodate the resulting convergence (Wang et al. 2001). As a consequence, the landscape is forced to adjust to the tectonic conditions. Thus, the interplay between rock uplift and erosion, which are the key processes, forms the topography of the orogen. Researchers found ways to use this dependency in order to recalculate the erosion (or rock uplift) from the topography. A powerful tool is the analysis of the morphology of river channels which has proved to be a robust proxy for the occurring erosion. The methods implemented in the early 20<sup>th</sup> century have been developed and improved to better constrain the underlying processes e.g. (Hack 1957, 1973; Whipple und Tucker 1999a). Today many researchers perform river network analysis to gain the steepness and the concavity index of channel segments for assumptions about the recent tectonic conditions e.g.(Whittaker 2012). For the Himalaya, a tremendous amount of studies has been published in order to explain the recent tectonic mechanisms responsible for the uplift of the orogen and some of them by using the mentioned indexes. e.g. (Ader et al. 2012; Bollinger et al. 2006; Lavé & Avouac 2000, 2001; Wobus et al. 2005; Wobus et al. 2006b; Whipple et al. 2016; Elliott, J. R. et al. 2016). The Central Himalaya is attractive in many ways for such researches. One benefit derives from the direction of the plate convergence which is perpendicular to the mountain front. Therefore the expected pattern of the deformation is simpler than in oblique, compressional zones additionally experiencing shear motion. Furthermore, the region in Central Nepal is favored for this kind of analysis because the setting is representative for a large area of the Himalaya. The classic geometry of the orogenic wedge contains four pronounced physiographic units separated by major fault systems (Fig. 1 & 24) Nevertheless, seismic sections are lacking for large parts of the Himalaya. Thus, geometries of faults and other structural features are still unknown. There is good reason that the subsurface is more differentiated and segmented than expected as shown by Harvey et al. (2015) suggesting changes in the geometry of the subsurface of the Central Himalaya via analysis of river networks.

According to the northwestern part of the Himalaya, previous studies already described topographies of the mountain front deviating from the classic build up. e.g. (Burbank 1983; Thakur 1998; Powers et al. 1998).

We have expanded the approach of the river network analysis to the northwestern Himalaya. We calculated the river steepness indexes for tributaries with a drainage area falling in a range

between 5 km<sup>2</sup> and 200 km<sup>2</sup>. We use this proxy for erosion in order to look for along strike changes in the thrust geometry and to assess the activity of fault segments as well as their contribution to the crustal shortening. The gained 2D-results display a coherent overview of the distribution of the erosion rate in NW India supporting an out-of-sequence activity of multiple fault segments. The expected tectonic activity of the MBT as well as of the PT2 promoting structure is variable along strike. These results improve the understanding of the ongoing orogeny and the accommodated deformation since the Pleistocene. Moreover it improves the understanding of the relationship between segments of different subsurface geometries.

## Geologic setting

### Tectonic evolution and recent setting

The Himalaya is the highest orogen on earth. As such, a lot of research has been done in order to understand the process of this tremendous rise as a consequence of the continental collision of the Indian and the Eurasian tectonic plate. The tectonic evolution of the Himalaya is roughly identical along the whole mountain range. After the closure of the Neotethys ocean the collision of the continental plates India and Eurasia started 55 Myr ago in the NW Himalaya (Thakur 1993) p.319. As a consequence, the northern margin of the Indian plate was deformed and its rocks underwent regional metamorphism resulting in the units of the Greater Himalaya. As a result of the continued convergence, the Main Central Thrust (MCT) has uplifted those metamorphic units above the formations of the Lower (or Lesser) Himalaya (Thakur 1993) p.6. The southern limit of the Lower Himalaya is set by the MBT (Main Boundary Thrust), which developed at least 10 Ma ago (Meigs et al. 1995). Lying in between the MBT and the MCT, the Lower Himalaya had been folded and underwent a low grade of metamorphism. This very continuous thrust fault has overridden the units of the Subhimalaya which mainly comprises of molasse material (Thakur 1993) p.5. Drillings have shown that these lithologic units reach far south into the Ganga basin (Powers et al. 1998; Mugnier und Huyghe 2006). This supports the theory of a continuous foreland basin. Due to the propagation of the orogenic wedge in the late Quaternary, the Main Frontal Thrust (MFT) has developed as the youngest in-sequence thrust of the Himalaya (Thakur et al. 2007; Thakur 1993) p.5. The Subhimalaya zone can be best described as a foreland fold-and-thrust-belt. The triplet of MCT, MBT and MFT, although deviating in distance to each other, can be found all along strike of the Himalayan orogen (Fig. 1).

In contrast to the Central Himalaya, previous studies observed that in the northwestern Himalaya the convergence direction is not perpendicular to the mountain front e.g. (Tapponnier und Molnar 1979; Kundu et al. 2014; Silver, Calvin R. P. et al. 2015). Thus, the oblique convergence results in strain partitioning where the arc-normal deformation is accommodated via thrusting along the main faults and a strike slip component which is accommodated in the orogen interior. One of the main agents accommodating the strike slip component and other exceptional feature in the NW Himalaya are described in more detail.

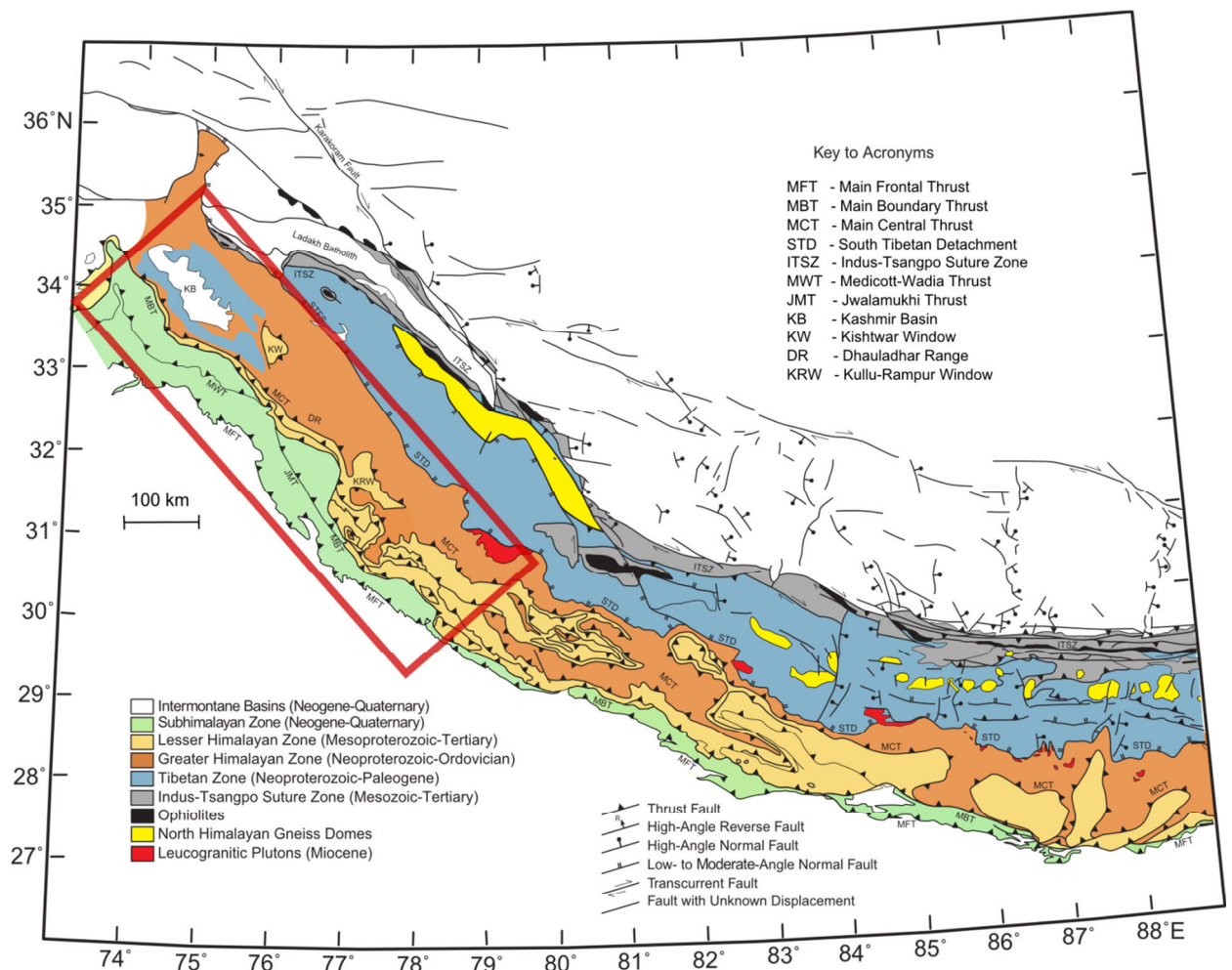


**Figure 1 Geologic map of the Western Himalaya.(modified from Hodges, 2000) The red rectangle bounds the study area of this thesis.**

### Karakorum-Fault

For the scope of this thesis, it is necessary to mention some regional fault systems which are only present in the north western part of the mountain front but may have an enormous effect on the tectonic evolution. The NW striking Karakorum fault is about 1000km in length and it is part of the contractional system in the western portion of the Himalayan-Tibetan orogenic belt. To the east, the oblique, dextral fault joins into the frontal thrusts of the

Himalaya. Its northern extension reaches into the Pamir orogen where it splays into dextral strike-slip and thrust faults (Strecker et al. 1995). Traced horizons like the Aghil-fm. cut by the fault revealed that the total offset of the Karakorum fault is between 149 km and 167 km (Robinson 2009a). According to performed GPS measurements, the fault rather pushes the southern Himalaya to the west than the Tibetan Plateau to the east (Banerjee 2002). Today's velocity based on GPS-data is still debated and ranges from  $1\text{-}4\text{mm}\cdot\text{yr}^{-1}$  (Banerjee 2002) to  $5\pm2\text{ mm}\cdot\text{yr}^{-1}$  (Kundu et al. 2014). However, the slip rate does not seem to be constant through the ages (Kundu et al. 2014; Banerjee 2002). Geological offsets expect rates of ca.  $11\text{mm}\cdot\text{yr}^{-1}$  since the Miocene (Robinson 2009a). Geomorphic studies using cosmogenic nuclide dating of offset moraine surfaces have presented velocities of  $\sim10\text{ mm}\cdot\text{yr}^{-1}$  (Chevalier et al. 2005). Due to the nature of this method, the rate is representative for the motion on a millennial timescale.

### Duns and Salients

In general, the collision of India and Asia resulted in parallel longitudinal ranges but looking closer the resulting thrust geometries in the northwestern Himalaya are slightly different. The MBT describes a rather sinuous trace in the NW part of the orogenic belt (Fig.1). In contrast, the NW striking MFT is rather straight. As a consequence of this difference the fold- and thrust belt changes its width and develops 'Duns' and 'Salients'. Outstanding is the Kangra Dun (or Punjab re-entrant) having a maximal width of ca. 140km between the MBT and the MFT. Thus, the Kangra Dun is the largest reentrant to be found in NW India. It is bounded by the Nahan salient to the south and the outlet of the Ravi River to the north. The occurrence of duns and salients is still not completely understood but previous studies suggest that the angle of the MHT is higher beneath a salient (Singh et al. 2012).

### Kashmir Basin

The Kashmir Basin is located northwest of the Kangra reentrant and is a rather exceptional feature in the structure of the Himalaya (Fig. 1). As already mentioned the MBT was formed at least 10 Myr ago (Meigs et al., 1995). This is also true for northwestern part of the Himalaya but the thrust had been displaced towards the southwest at least 4 Myr ago and uplifted the southwestern margin of the basin, the Pir Panjal Range (Burbank & Johnson, 1982), (Burbank 1983). The active mountain front propagated further when the Medicott-Wadia-Thrust and the Suruin-Mastgarth Anticline developed, most likely since 2 Ma (Burbank et al. 1986). The northeastern margin of the Kashmir Basin is set by the Greater Himalayan Range (Burbank & Johnson, 1982).

## Description of physiographic units

### Tethys Himalaya

The Tethys Himalaya Zone is a metasedimentary layer on top of the Higher Himalayan metamorphic rocks with a maximal thickness of 10km. The marine sediments have been deposited between the late Precambrium to the Lower Eocene on a shelf or marine slope, the former northern passive margin of India (Thakur, 1993) p. 149. This enormous time span gave enough opportunity to deposit different kinds of siliciclastic and calcareous sediments. The zone is present from the Zanskar Mountains in the west along the whole southern margin of the Tibetan plateau (Thakur 1993) p.6. It is also known as the Tibetan Zone or Tibetan Himalayan Zone.

### Higher Himalaya

The crystalline band of the Higher Himalaya was uplifted via the MCT. Due to barrowvian metamorphism during early stages of Himalayan crustal thickening, rocks varying from green schist to highest amphibolite facies and migmatites are the most common (Thakur 1993) p.107. In addition, granites, granitoids and orthogneisses are also common because of several intrusive events in the Cambrian and in the Tertiary (Thakur 1993) p.107.

### Lower Himalaya

Proterozoic to Eocene rocks, covering the basement of the Indian craton, which have been detached by the underthrusting of the Indian plate and incooperated into the Himalayan orogenic wedge build the units of the Lower (or Lesser) Himalaya. They underwent a lower grade of metamorphism. It is mainly made of low grade metasediments. Sheared sediments like phyllites and schists but also calcareous rocks are common. Nevertheless, the erosional resistivity of the material is lower compared to the crystalline rocks of the Higher Himalaya.

### *Subhimalaya*

Completely unmetamorphosed, sedimentary rocks describe this sequence. It is limited by the MBT in the north and by the MFT to the south. The including formations have been continuously deposited in front of the whole mountain range. The first units of the Subathu group, marking a marine transgression and thus the closure of the Neotethys, were formed in the Upper Paleocene (Thakur 1993) p.20. Due to the shallow marine environment mainly fossil-bearing shales and limestones had been deposited (Thakur 1993) p.20. Since the late Eocene, the Dharamsala group follows in the area of Himachal Pradesh. This group is divided into two subgroups, the Lower and the Upper Dharamsala which have been deposited at the beginning of the Miocene. The Lower Dharamshala is characterized by “purple clays, siltstones and greenish grey and red clays”(Thakur 1993)p.20. Due to the rising supply of coarser

terrestrial material into the depositional environment during the continued orogeny, the Upper Dharamsala contains more “sandstone with minor amounts of greenish grey and red clays”(Thakur 1993) p.20. The upward coarsening trend continues in cycles through the Siwalik groups. The Lower Siwalik contains alternations of sand- and claystone. Some horizons contain limestone, quartzite and sandstone clasts (Thakur 1993). The Middle Siwalik mainly consists of sandy, arkosic litharenites alternating with minor claystone layers. Alternation with pebbly conglomerates can be observed in the upper part. The Upper Siwalik units have been deposited from the Pliocene to the Pleistocene. They are made of polymictic, boulder conglomerates with the occasional occurrence of sand lenses. According to my observations in the field, the cementation of single beds alternates. In general, well cemented conglomerates can rather be found in the lower part of the group. The youngest formation is the Neogal. The sediments of this unit fill the piggy back basins of the internally deformed Siwalik units. The majority of the sediment supply of the Kangra basin derives from the Dhauladhar range which is mainly made of granitoid rocks. Thus, the alluvial fan deposits in front of the range and other filling material are made of monomictic conglomerates with a minor amount of mobilized clasts from the Siwalik group. These beds are usually less cemented than the Upper Siwalik beds.

### Theories for the accommodation of the crustal shortening

In the most classical structure of the Himalaya which is representative for large areas of the orogen, the four physiographic units, described above, are bounded by major fault systems (Fig. 1) (Gansser A. 1964), (Hodges 2000) and references therein). Our understanding and structural constrain of the geometry of the Himalayan thrust system throughout the entire orogen is still loose. The knowledge about the exact depth or location of major fault geometries and the magnitude of slip rates at major fault systems are still strongly debated. One of the most obvious topographic features has been the pronounced change in the topography, and steepened longitudinal river profiles along the transition between Lesser and Higher Himalaya (e.g Seeber & Gornitz 1983; Wobus et al. 2005). Therefore, the Central Himalaya has been in the focus of many studies explaining the physiographic transition between the Lower and the Higher Himalaya and how the convergence between the Indian plate and Eurasian plate is accommodated. Their structural architecture mostly agrees in terms of a ramp structure along the MHT (Fig. 2). However, three theories have developed explaining the deformation along the MHT. The first scenario is characterized by in-sequence thrusting (Fig. 2A). Here, the total amount of shortening is accommodated at the MFT (Lavé & Avouac 2000). This had been observed south of the Kathmandu Basin. The study determined the incision rate of the Bagmati and the Bajura River to infer the necessary rock uplift rate of

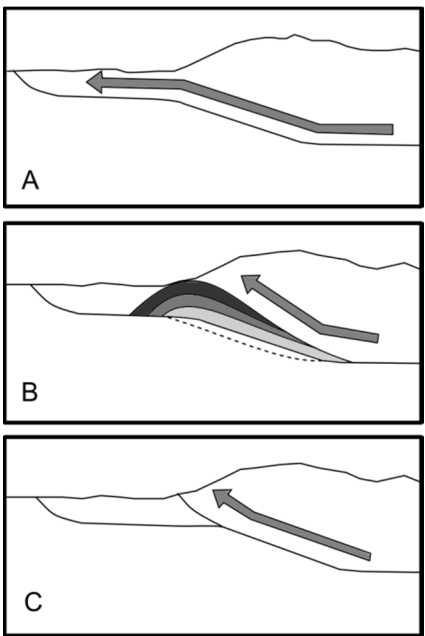


**Figure 2.** The simplified models illustrate three different concepts of how the tectonic convergence is accommodated at the Himalayan front. (Figure modified from Wobus et al., 2006) Model A) Rock uplift around the PT2 is the result of material transport over a mid-crustal ramp. (Lavé & Avouac, 2000) Model B) Accretion of the footwall into the hanging wall forms a passive duplex structure accommodating the shortening (Bollinger et al. 2004; Wobus et al. 2006, Elliot et al. 2016). Model C) Active out-of-sequence thrusting results in uplift of the Greater Himalaya (Wobus et al., 2005; Whipple et al. 2016)

the MFT. They claim that the MHT entirely ruptures at once resulting in very large earthquakes. The change in topography and relief at the PT2 is solely caused by the slip of the Eurasian plate over a mid-crustal ramp (Lavé & Avouac 2000; Herman et al. 2010). The second scenario explains the pronounced deformation around the PT2 by presence of a duplex structure developing by accretion of the Indian crust into the Himalayan wedge (Fig. 2B) (Bollinger et al. 2006),(Caldwell et al. 2013),(Gao et al. 2016). This is supported by the distribution of  $^{40}\text{Ar}/^{39}\text{Ar}$  cooling ages (Wobus et al. 2006b). The third scenario takes into account that out-of-sequence thrusting occurs along the PT2 (Fig. 2C) (Wobus et al. 2005). In the course of the discussion we will interpret our results with respect to those theories and different structural settings to examine the tectonic convergence in the northwestern Himalaya.

### Direction and velocity of plate motion

Considering Eurasia as a fixed reference point the center of the Indian craton (GPS -station IISC in Bangalore) moves at a rate of  $37 \pm 1 \text{ mm/yr}$  towards NNE (Wang et al. 2001). The analysis of GPS-measurements along the Himalaya range and in the Tibetan plateau revealed that the recent convergence is accommodated by multiple fault systems (England & Molnar 1997),(Wang et al. 2001). Furthermore, the convergence rates tend to decrease from the eastern to the western part of the mountain belt (Banerjee 2002; Stevens & Avouac 2015) and references in there). Geomorphological and structural studies have shown coincidentally that shortening rates in the western parts of the mountain front are about  $14 \pm 2 \text{ mm yr}^{-1}$  (Powers et al. 1998) which is about 20% less than in central Nepal (Lavé & Avouac 2000; Kundu et al. 2014).

The reconstruction of the Indian plate motion showed that India's direction and velocity has changed during the last 20 Myr (Molnar & Stock 2009). Its rotating motion has changed the

direction from 10°N to 20°N and thus became clockwise (Molnar & Stock 2009). Moreover the convergence rate decreased from 44 to 34mm·yr<sup>-1</sup> in NW India (Molnar & Stock 2009) which is comparable with the latest results from Wang, 2001.

## Seismic activity and geodetic velocities in NW India

In order to give a brief overview about the seismo-tectonic setting in the study area we use the seismic data from the NEIC catalogue (Fig. 3). This catalogue includes historic events since 1905 and a continuous record since 1973 for earthquakes with a moment magnitude larger than 3. The data reveal that the majority of the earthquakes in the southern part of the study area are located around the PT2. However, the amount of events decreases following this structural feature to the northwest. Just few events can be determined around the Kullu-Rampur Window. North of the tectonic window we see a large cluster of seismic events. Unfortunately, we have no information about the focal mechanisms but these events are assumed to belong to the extension in the Kaurik Chango Rift (Arora et al. 2012). Another noticeable accumulation of seismic events occurring on thrust faults can be seen around the Dhauladar Range and at the southern border of the Kishtwar window. Looking again further to the northwest just few events can be observed in the study area. The sparse amount of events is mainly located in the Kashmir Basin. In general, most of the events are located northeast of the MBT. Just very few events can be observed in area of the Subhimalaya.

The GPS velocities taken from a study of Banerjee, et al. draw a similar picture. The highest rates are measured by GPS stations in the hanging wall of the MBT (Banerjee et al. 2008). They fall in a range between 4-18 mm/yr while the lowest rates are measured by stations the southern study area. However, the velocities measured by stations in the Subhimalaya are seismically locked and therefore the slowest. They range between 0.5 and 4 mm/yr (Fig. 3).

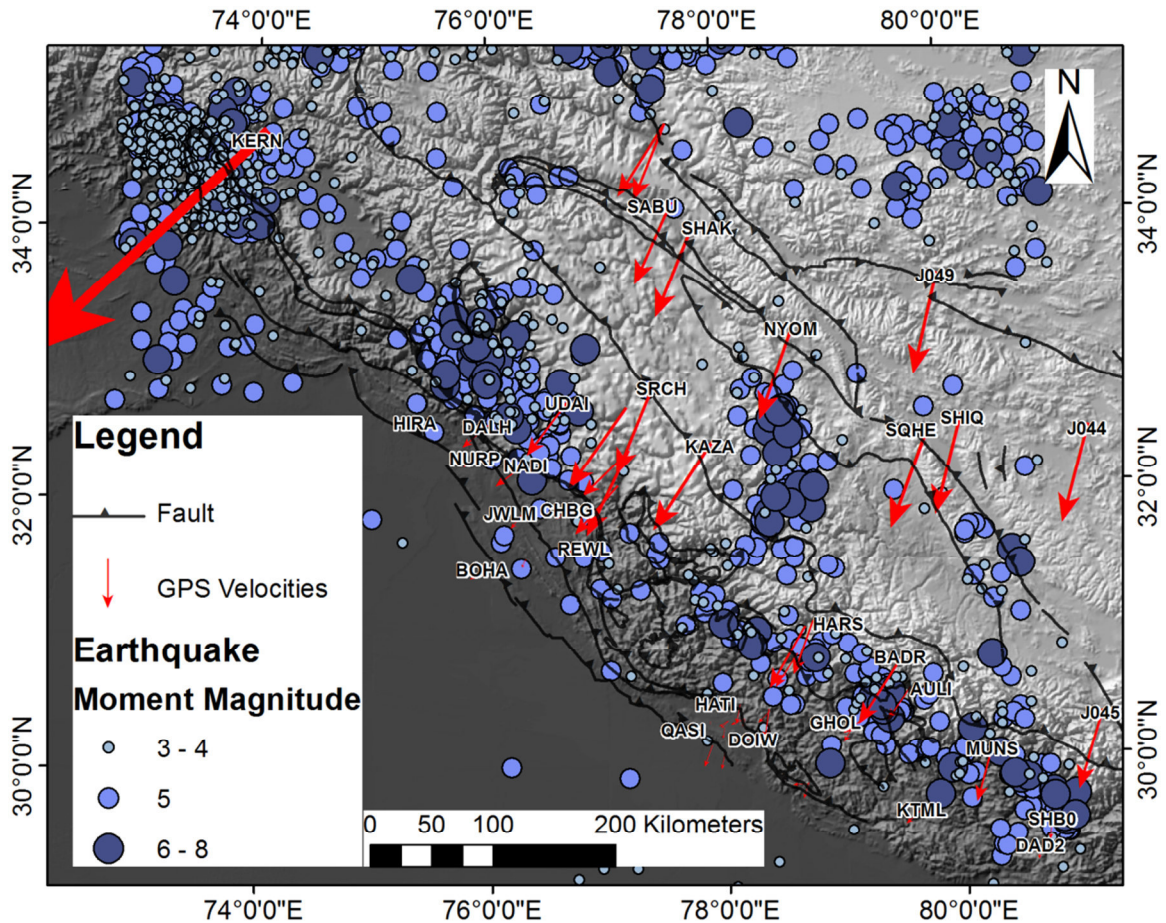


**Figure 3. Location and magnitude of seismic events from 1905 to 2016 with continuous record since 1973 (from NEIC catalogue). Moreover, red arrows illustrate the annual shortening rate measured by GPS stations in the northwestern Himalaya. (data from Banerjee et al., 2008).**

These data show that we already have a good idea about how the recent convergence is accommodated in the Himalayan fault systems. However, these datasets cover a very short time span and do not include large seismic event with long recurrence times. Furthermore, we do not know which fault or fault segment accommodates the main shortening. Even if we determine the location of earthquake epicenters we cannot necessarily determine the ruptured fault. This is crucial for the understanding of the evolution and the propagation of the orogenic wedge. We use geomorphological methods in order to integrate the tectonic evolution over a larger period and to solve this lack of information.

## Methods

### River steepness and concavity index

The profile of a river is the result of many environmental influences. Key factors responsible for its shape are tectonic and climatic conditions. Additionally, the profile shape strongly depends on the bedrock or underlying substrate, the most effective erosion process, the channel depth and width, the specific discharge and the periodicity of events. Because the complete erosional processes acting on a river basin are difficult to separate and quantify, many models use an empirical approach to describe fluvial erosion as a power law function of upstream area and channel slope. This approach is based on the assumption that erosion is primarily controlled by bed shear stress (Whipple & Tucker, 1999). The relationship between erosion, upstream area and slope can be approximated as follows:

$$E = KA^m S^n$$

(Eq. 1) by Whipple and Tucker, 1999

This stream-power equation describes the erosion ( $E$ ) for a specific point in the river channel as a function of the erosion coefficient ( $K$ ), the upstream area ( $A$ ) which serves as a proxy for discharge ( $Q$ ) (Whipple & Tucker, 1999) and the channel slope ( $S$ ) which is used as a proxy for erosional efficiency. The exponents  $m$  and  $n$  are scaling factors related to the hydraulic geometry, basin hydrology and erosion processes (Whipple & Tucker, 1999). Whipple and Tucker calculated that typical hydrological values result in a  $m/n$  ratio varying between 0.35 and 0.6 (Whipple & Tucker, 1999). By using Eq. 1 in combination with a known rock uplift rate  $U$ , we can calculate the surface uplift rate (England & Molnar 1990).

$$\frac{\delta z}{\delta t} = U - E = U - KA^m S^n$$

(Eq. 2) by Whipple and Tucker, 1999

In areas of topographic steady state, where the erosion rate equals the rock uplift rate, the surface elevation remains steady. Thus, Eq. 2 can be simplified and rearranged for the channel slope. For each point in the river profile, this equilibrium slope is described by the following equation:

$$S = k_s A^{-\theta}$$

(Eq. 3) by J.T. Hack, 1957 and J.J. Flint, 1977

Here,  $k_s$  is the steepness index, resulting from  $(U/K)^{1/n}$  (Wobus et al. 2006) and  $\theta$  as the concavity index, which is equivalent to the  $m/n$  ratio.

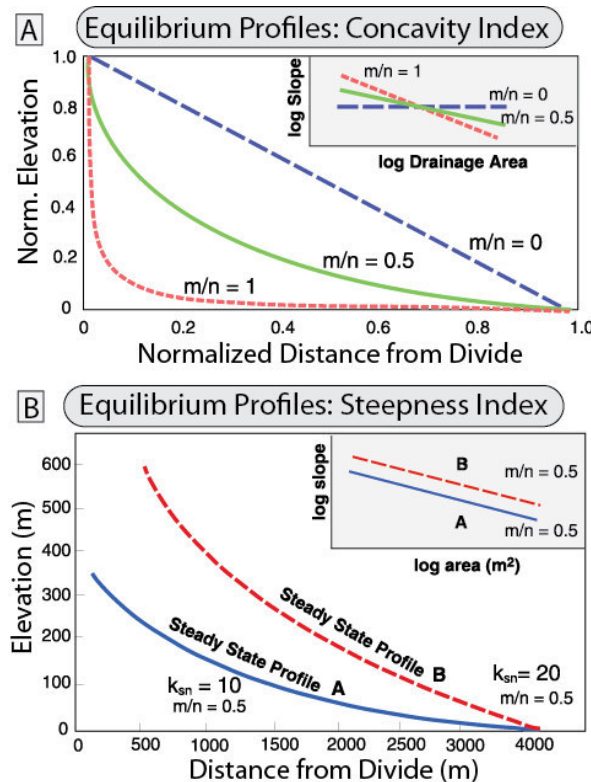


**Figure 4.** Figure A and B schematically show the concept of the normalized steepness index and the concavity index in an elevation vs. distance plot and in a logarithmic slope vs. area plot. In the upper figure, the steepness index is fixed but  $\theta$  ( $m/n$  ratio) varies between 0 and 1. The figure below presents two longitudinal profiles with different  $k_{sn}$  values. The concavity index is 0.5 for both profiles. (from Kirby and Whipple, 2012; Duval et al., 2004; Whipple and Tucker, 1999)

calculated from  $m$  and  $n$  values by Whipple and Tucker in 1983. However, the indexes  $k_s$  and  $\theta$  commonly increase in areas with a high rock uplift rate, and even small variations in the concavity index can have strong effects on the  $k_s$  value (Wobus et al. 2006a). This makes it difficult to compare multiple river profiles with each other, however, because concavity falls in a relatively restricted range it is acceptable to normalize it by a reference concavity often

In order to estimate steepness indexes and concavity indexes for a specific river segment, a linear regression in a log-log plot of channel slope and catchment area can be used to determine  $k_s$  and  $\theta$  (Kirby & Whipple 2012; Whittaker 2012). The longitudinal profiles for various combinations of  $k_s$  and  $\theta$  can be seen in Figure 4.

A significant number of studies have confirmed the positive relationship between rock uplift rate  $U$  and river steepness  $k_s$  (e.g. Wobus et al. 2006a, Kirby & Whipple 2012 (and references

therein). On the contrary, the concavity  $\theta$  is rather insensitive to uncertainties in rock uplift rate, climate and bedrock lithology (Wobus et al. 2006a; Kirby & Whipple 2012). Many studies observed concavity indexes ranging between 0.4 and 0.6 in settings with uniform conditions (Kirby & Whipple 2012).

These values fall in the same range

taken as  $\theta_{ref} = 0.45$  (Wobus et al. 2006a). The normalized channel steepness equation then becomes.

$$S = k_{sn} \cdot A^{-\theta_{ref}} \quad (\text{Eq. 4})$$

## Knickpoints in longitudinal river profiles

The assessment of steepness patterns along river profiles has to take temporal and spatial uncertainties into account. Nonlinearities in the incision process, adjustments in the river's morphology, changing bedrock settings, enhanced perturbations by hillslope processes and orographic influences on the precipitation pattern can perturb the steepness pattern (Kirby &

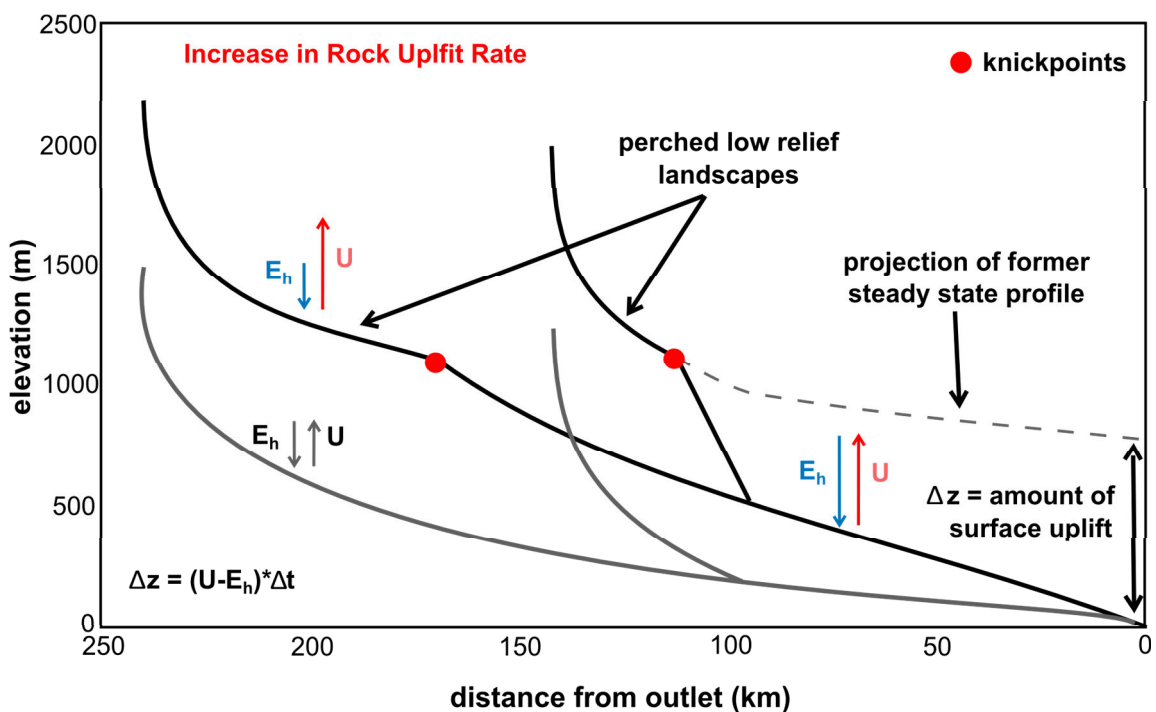


**Figure 5.** The graph schematically shows a longitudinal river profile in a transient state (black line). The grey lines present the former steady state profile or its projection. The knickpoint originates from a change in the base level elevation. Here, this change is caused by an increase in the rock uplift. The resulting disequilibrium between erosion rate and uplift rate leads to an upstream migration of a knickpoint. In this figure, the concave knickpoints ideally are at the same elevation. (from Kirby and Whipple, 2012)

Whipple 2012). In general, the channel slope will always adjust to its current downstream base level. That is why rivers in a transient state will respond to temporal changes by knickpoint development and migration (Kirby & Whipple 2012) until a new equilibrated state is reached. A schematic example is shown in Figure 5. Here we see a river in a transient state adjusting to a new setting with an increased rock uplift rate. The amount of erosion in the downstream part is already adapted to keep pace with the accelerated rock uplift. Due to

headward erosion a knickpoint originates and migrates upstream until the complete profile is in equilibrium to the new setting. Thus, the identification of such knickpoints is crucial for the determination of the river system's condition.

In order to determine knickpoints along a profile from digital elevation models (DEMs) it is helpful to create chi-plots (Royden & Perron 2013). The advantage of the chi-plot procedure is that the concavity of the stream is removed by an integration of the stream power equation, which also removes the need to calculate slope from noisy elevation data. Chi-plotting collapses the stream profile to a straight line and maximal deviations from this regression can be identified as knickpoints in the stream profile.

Despite the straightforward procedure for identifying knickpoints, determining their origin can be more difficult. As to be seen in Trans-Himalayan-rivers, multiple faults can create a continuous but differential uplift causing rivers to develop knickpoints (Seeber & Gornitz 1983). In contrast to the knickpoints mentioned above, it is assumed that these irregularities have fixed locations as long as the differential uplift is active. Moreover, similar profile anomalies can also appear at lithologic contacts if the difference in the substrate's resistivity is high. Because of that, it is crucial to include structural and geologic maps as well as known shortening rates for a reasonable interpretation.

## Processing the channel steepness indexes

The river channel analysis was carried out with a Matlab-based script developed by Bodo Bookhagen and Alexander Neely using functions from the Topotoolbox module by W. Schwanghart and the Chi-plot algorithm for the knickpoint localization by L. Royden and J.T. Perron (Schwanghart & Scherler 2014), (Schwanghart & Kuhn 2010), (Royden & Perron 2013).

Topographic calculations were performed with the SRTM 1 arc second DEM (data available from U.S. Geological Survey) with a spatial resolution of 30m. All data were projected in the WGS 1984 UTM zone 43N ranging from 72°E to 78°E in the northern hemisphere.

Matlab based calculations were run to obtain properties of the longitudinal river profiles. They were carried out in a batch mode for every stream in the study area with a minimal drainage area of 1km<sup>2</sup> (see input parameters). This threshold has often been documented as the transition between the colluvial dominated and the fluvial dominated regime. Thus, the area upstream of this threshold has not been involved in the calculation in order to avoid signals biased by hillslope processes (e.g. landslides).

The code separates the longitudinal stream profile into multiple segments of a predefined length. Thus, the steepness of each channel segment is calculated with its upstream catchment area respectively. Input parameters used for the calculation are given in the appendix (see input parameters).

## Post-processing steepness indexes

### Correction for glacial erosion

Channel steepness is an appropriate indicator for the amount of erosion in fluvial dominated regimes. However, the northwestern part of the Himalaya is partially covered by glaciers. The erosive process as well as the erosional efficiency in these areas deviates from fluvial erosion. For that reason, the data was cleaned for regions where glacial erosion is dominant by mapping terminal moraines on satellite images from Google Earth® and combining them to glaciated areas (Fig. 6). The resulting features were used as clipping agents and the associated stream features were excluded from further calculations (Fig. 7).

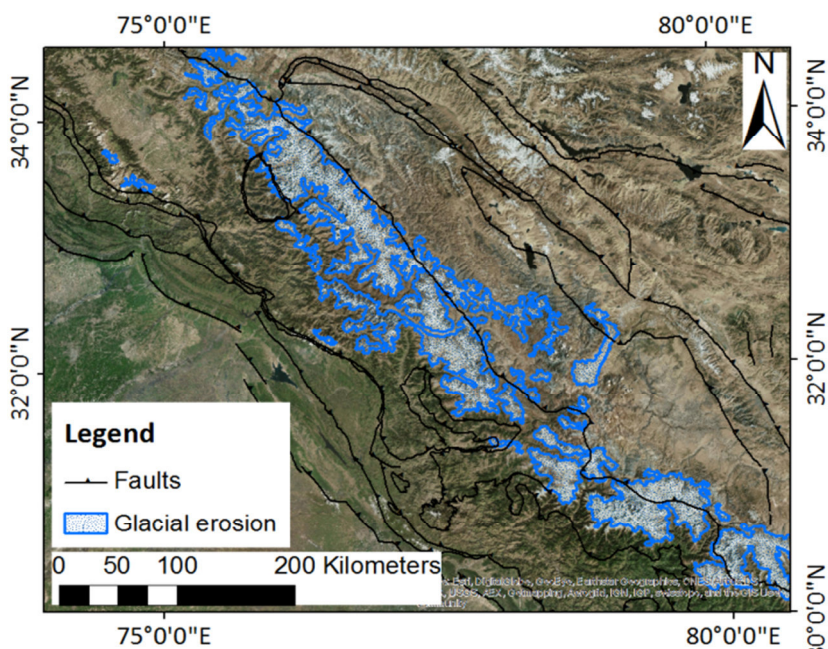
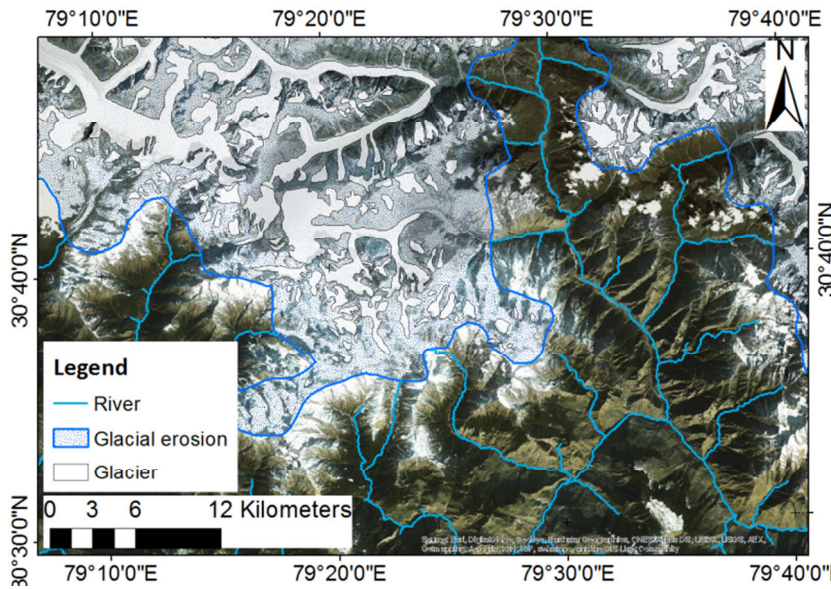


Figure 6. This figure shows the mapped regions in the study area which are dominated by glacial erosion. This map uses the "World Imagery" basemap by Esri, DigitalGlobe, GeoEye, I-cubed, USDE FSA, USGS, AEX, Getmapping, Aerogrid, IGN, IGP, swisstopo, and the GIS User Community

### Catchment-wide steepness index

We determine all catchments in the study area with a Strahler stream order of 3 (drainage area 5- 250km<sup>2</sup>). These catchments are considered drainage basins of tributaries. This fact is helpful because knickpoint migration is much slower in streams with a low erosion-rate. With regard to eq.1 we can say that in uniform settings a smaller drainage area leads to less erosion. Thus, knickpoints indicating an environmental change are stored in tributaries for a longer period of time (Whipple & Tucker, 1999).



**Figure 7.** After processing the steepness index of the channel segments we clipped the stream network for areas where the glacial morphology is dominant. Therefore we searched for terminal moraines in satellite images and combined them to disregard areas. This map uses the “World Imagery” basemap by Esri, DigitalGlobe, GeoEye, i-cubed, USDE FSA, USGS, AEX, Getmapping, Aerogrid, IGN, IGP, swisstopo, and the GIS User Community

The obtained  $k_{sn}$  values ( $\theta_{ref} = 0.45$ ) of all stream segments within a catchment were averaged and assigned to the catchment. The output of this procedure is a map showing the tributary catchments in the NW Himalaya with averaged  $k_{sn}$  values. This visualization is used in order to improve the graphical representation of the  $k_{sn}$  values. Furthermore the method has the advantage that it presents the output of the calculation on the sub-orogenic scale while preserving the fluvial character of the parameter.

## Hot Spot Analysis

We run a hot spot analysis, in order to identify regions in the orogen with a significant amount of catchments sharing similar steepness indexes. This calculation has been performed including all catchments inside the study area. The analysis determines whether the occurrence of steep and/or gentle channel profiles in a specific perimeter is significant or not.

## Topometric analysis

Landscape morphology provides information about surface and subsurface processes. Topographic analysis includes the investigation of topographic metrics, which can reveal first-order patterns of active tectonics. We performed our analysis to infer relative changes in the surface uplift and the accumulated strain in the orogen. Therefore ten swath profiles were generated trending perpendicular to the strike of the northwestern Himalayan front (Fig. 8).

## Orthogonal swath profiles

Ranging from the Dehra Dun reentrant to the Kashmir Basin the locations of the profiles have been chosen in such a way to represent the major compressive regimes and variations within them. Those were the Dehra Dun reentrant, the Nahan salient, the Kangra reentrant, the area between the outlet of the Ravi and the Chenab and the area around the Kashmir basin. The

ten transects reach from the MFT to a point 200km in the hanging wall of the MBT. The width of the profiles is 20km (Fig. 8).

These profiles are used to present the distribution of steepness indexes as well as the

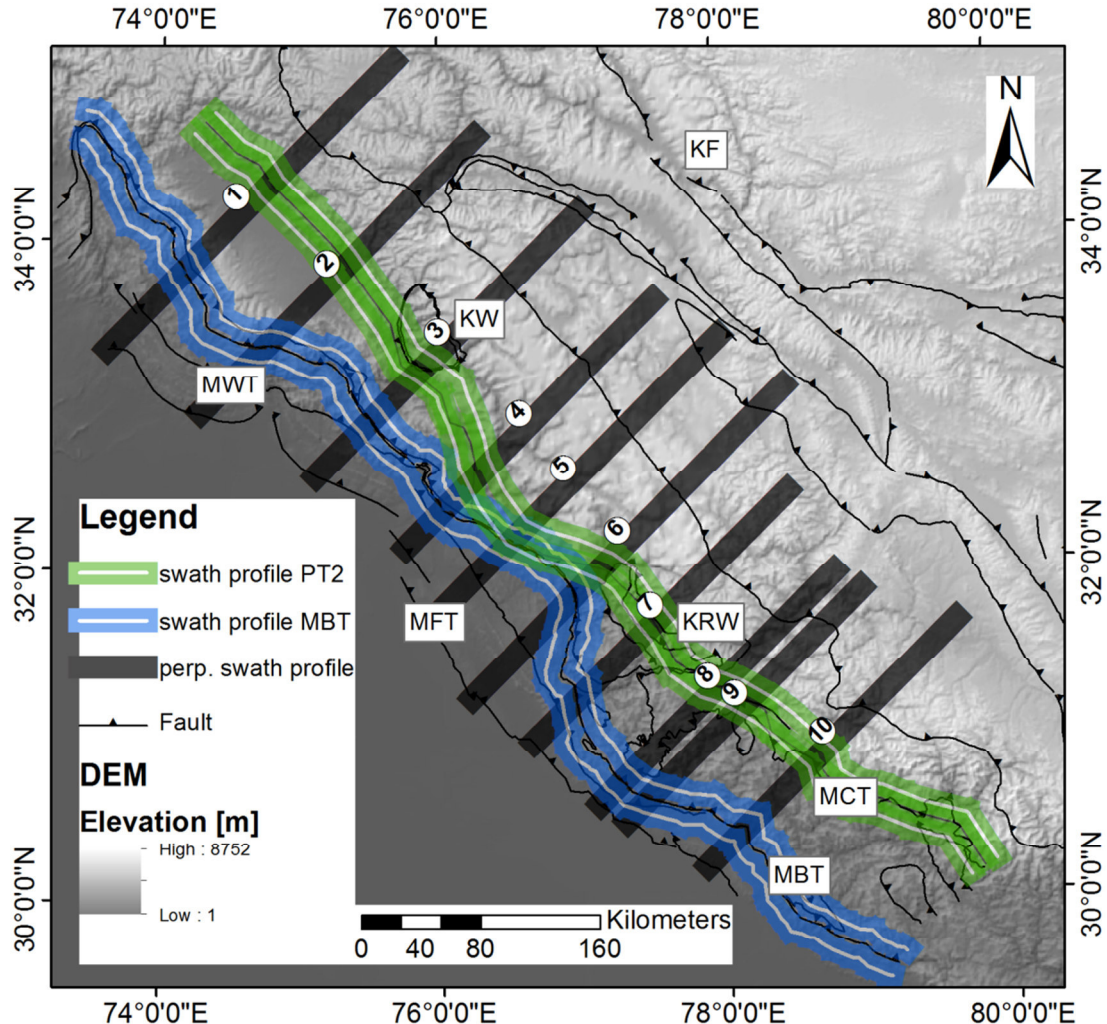


**Figure 8.** Beside the topography and the main faults in the northwestern Himalaya, this map shows the location of the swath profiles used for the topometric analysis. Profiles 1-10 strike 45°E. Thus, they are perpendicularly oriented to the orogen. Every profile starts at the MFT and reaches to a point 200km NE of the MBT. In addition, we respectively created two profiles parallel to the MBT and the PT2 to observe along strike variations in our parameters. KF: Karakorum Fault; KRW: Kullu-Rampur-Window; KW: Kishtwar Window; MFT: Main Frontal Thrust; MBT: Main Boundary Thrust; MCT: Main Central Thrust; MWT: Medicot-Wadia Thrust

elevation pattern and cumulative height. The cumulative height is the cumulative sum of the elevation at each point along the profile and it is used as a first order proxy for the accumulated strain within a specific distance.

### Parallel swath profiles

In addition to the orthogonal profiles, we have created profiles which run parallel to the MBT and to the PT2 (Fig. 8). Because the Main Boundary Thrust is well mapped, we have used the frontal most expression of the fault from the literature.

Unfortunately, the PT2 cannot be discretized by a single structural feature because it stays blind in the subsurface. The PT2 often, approximately coincides with the location of the Main Central Thrust (MCT). However, it is widely accepted that the MCT is a recrystallized Early Miocene ductile shearzone, but today inactive. The physiographic transition derives from a structural feature that underlies the MCT (Seeber & Gornitz 1983, several author relate the location of the PT2 to the existence of a steepen ramp segment with the MHT. Therefore, we have defined the location of the PT2 based on its expression at the surface, which is a vast, along strike increase in the topographic relief at the orogenic front. Areas with a relief higher than 2500m in a 10x10km window are located in the hanging wall of the structure. In the northwestern part of the study area (north of the Kashmir Basin) we used a relief of 2000m in a 10x10km window to define the PT2.

In the next step we created two parallel lines with an offset of 10km to the faults, one in the hanging wall and one in the footwall of each structural feature. The swath profile analysis has been performed along these four parallel lines. The width used for the swath profiles is 20km (Fig. 8).

The reason for this procedure is the following. In order to determine the location of an active fault segment, we create two swath profiles, one covering the hangingwall and one covering the footwall with respect to the expected location of the structural feature. By looking at the changes in the difference in channel steepness between the hanging- and the footwall, we can identify whether erosion is different in the hangingwall of a structure. In case of a high, positive difference we expect this segment to be tectonically active. On the contrary, segments with a low or even negative difference in the channel steepness are assumed to experience less fault displacement via the respective structural feature.

## Results

### Channel steepness in the NW Himalaya

Analysis of topography reveals the distribution of the channel steepness index in the northwestern Himalaya (Fig. 9). The study area covers a 400 km long strike-parallel segment of the southern Himalayan front in northwest India, covering all four major tectono-physiographic compartments of the orogen, the Subhimalaya, the Lesser Himalaya and the High Himalaya as well as the Tethyan Sequence from the Kashmir Basin in the northwest to Garwhal in the southeast. Being aware that the rock resistivity to weathering and erosion is not equal across these physiographic units, we have separately analyzed the catchments for each compartment. A detailed distribution of the channel steepness in each physiographic

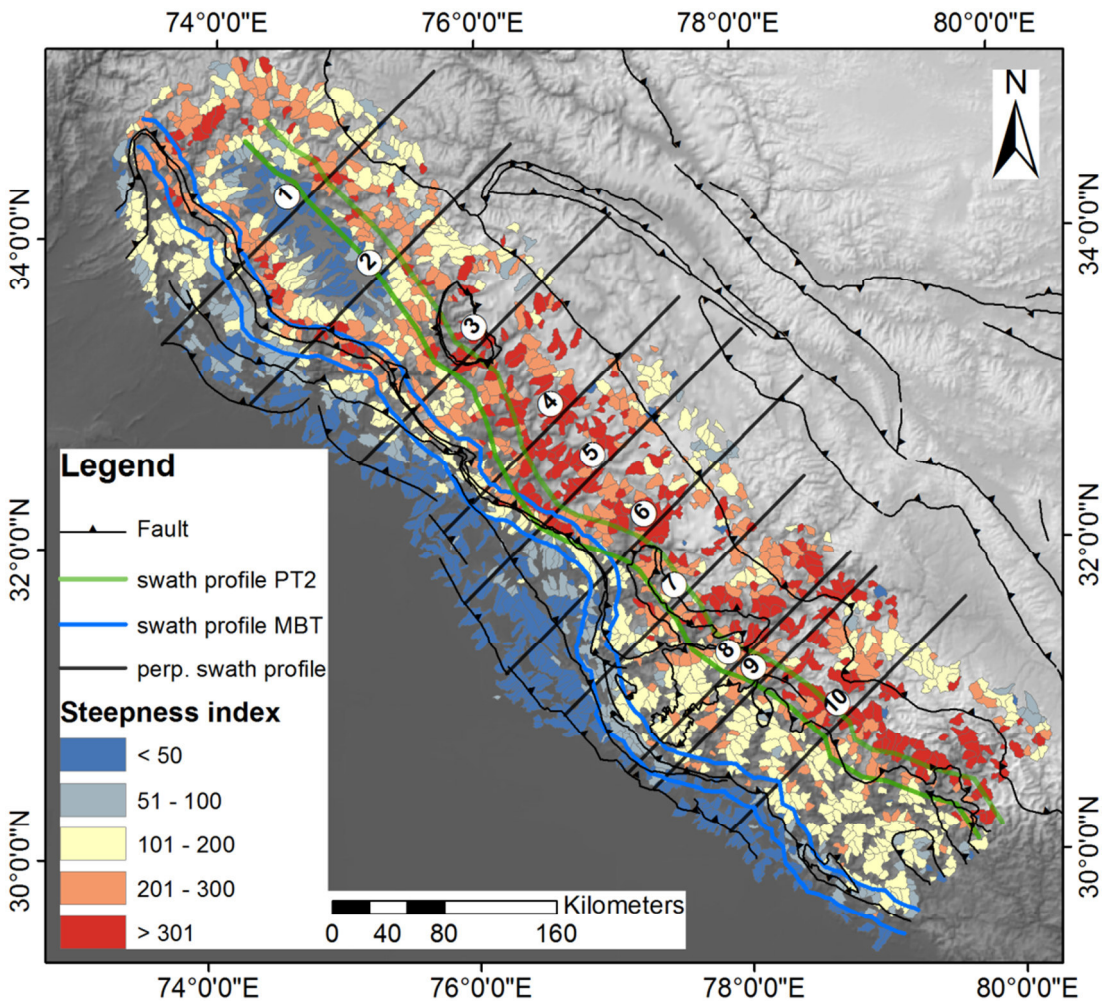


Figure 9. The focus in this map is on the distribution of the steepness indexes averaged over their drainage areas. Additionally, we can see the trace of the swath profiles 1-10 (dark grey) as well as of the profiles running parallel to the MBT (blue) and the PT2 (green)

unit is given in the appendix (see Steepness Index Histograms). However, first order signals on this scale can already be observed even if we not differentiate between the physiographic units. According to the distribution of the steep channel catchments, we divided the study area into three different regions along strike (A1-A3). In the southeastern part of the study area, we note a narrow band with low steepness indexes in the Subhimalaya ( $k_{sn} < 50$ ), a broad range with intermediate values in the Lesser Himalaya ( $k_{sn} = 100$  to  $k_{sn} = 200$ ) and very high values in the High Himalaya ( $k_{sn} > 200$ ). This part of our study area will be area A1. Area A2 comprises the Kangra reentrant, the Dhauladhar range and its hinterland, where regional pattern of topography suggest substantially differences from area A1. The Subhimalaya is wider but also comprises gentle river channels. The Lesser Himalaya is very narrow (<5km in width) in this area, therefore it is usually not recognized. The catchment  $k_{sn}$ -indexes drastically increase in the hangingwall of the MBT ( $k_{sn} > 300$ ). It is noteworthy that the prolongation of the band with high steepness index from the first area directly points to the location of the Dhauladhar range. This observation is key for the differentiation between A1 and A2 because such high steepness indexes are not associated to the MBT in A1. Area A3 is located in the northwestern part of the study area. We observe low to intermediate steepness indexes in the Subhimalaya ( $k_{sn} = 50$  to  $k_{sn} = 200$ ). In contrast to Area A1, just few catchments with  $k_{sn}$  indexes over 300 are located in the hangingwall of the MBT. However, the main contrast to A1 and A2 are the gentle channel profiles (( $k_{sn} < 50$ ) in a large intramontane basin, the Kashmir Basin. It is worth mentioning that there is a second area northeast of the basin where catchments are characterized by steeper river channels ( $k_{sn} > 200$ ). In order to differentiate these 3 settings in more detail, we created 10 swath profiles, which will be shown in the following.

## Description of the perpendicular swath profiles

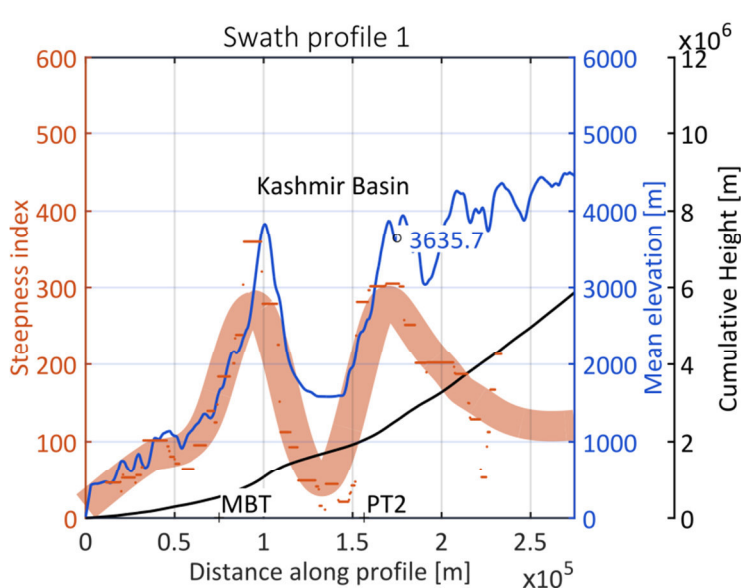


Figure 10. Profile 1

Plotted along the ten swaths are the averaged steepness of each catchment, the mean elevation profile and a profile of the cumulative height. We include a fitting curve showing a smooth trend of the distribution of the steepness indexes. In addition, we plotted the location of the MBT and the

PT2 as well as other important structural and geological features in each figure for orientation purposes.

### Profile 1 & 2

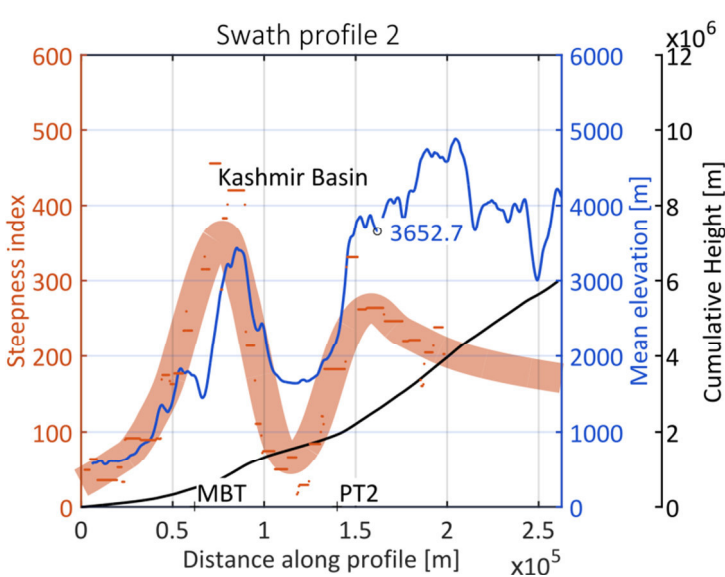


Figure 11. Profile 2

Profile 1 & 2 are the northwestern profiles crossing the Pir Panjal Range and the Kashmir Basin (Fig. 10&11). The topography in the footwall of the MBT increases steadily to ca. 1500m before crossing the MBT-thrust in both profiles. In both profiles, the topography of the Pir Panjal Range rises to over 3.3km in mean elevation before it

decreases towards the intramontane Kashmir Basin. The Kashmir Basin is characterized by a flat topography and mean elevation of around 1600m. The topography in both profiles rises again to elevations of 3.6km around the location of the PT2 and remains high for the rest of the profiles. At a distance of 100km to the MBT, the elevation falls in a range between 3635 m and 3652 m. The  $k_{sn}$  values roughly follow the same trends as the elevation patterns. The  $k_{sn}$  indexes in the footwall of the MBT fall in a range between 30 and 150. They show an increasing trend towards the fault. At the location of the MBT, we observe steepness indexes over 350 in profile 1. In profile 2 this first peak is around 450, which is interesting because we see a higher steepness index coinciding with a lower elevation compared to profile 1. The  $k_{sn}$  indexes decrease to values below 50 in the Kashmir Basin before they increase again near the PT2. Here we can observe another difference in the two profiles. In profile 1, we see that both peaks in the channel steepness distribution along the profile are comparatively equal while in profile 2 we identify higher steepness indexes around the MBT than around the PT2. Moving further along the profiles, the channel steepness decreases in both profiles, while the mean elevation stays high.

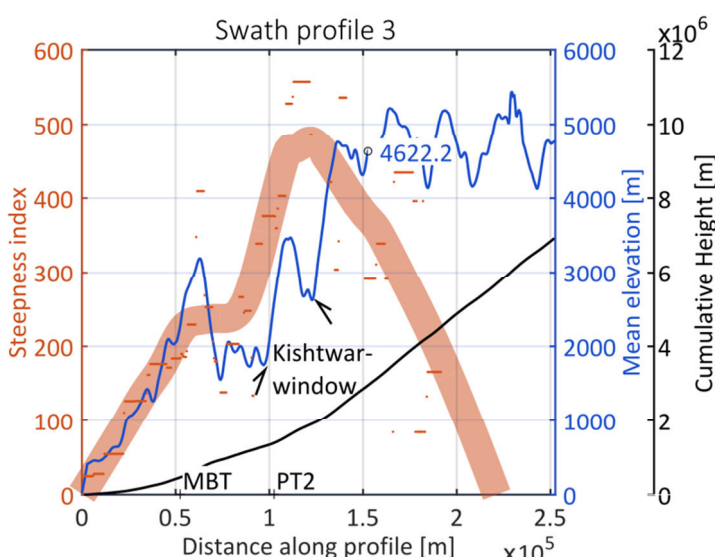
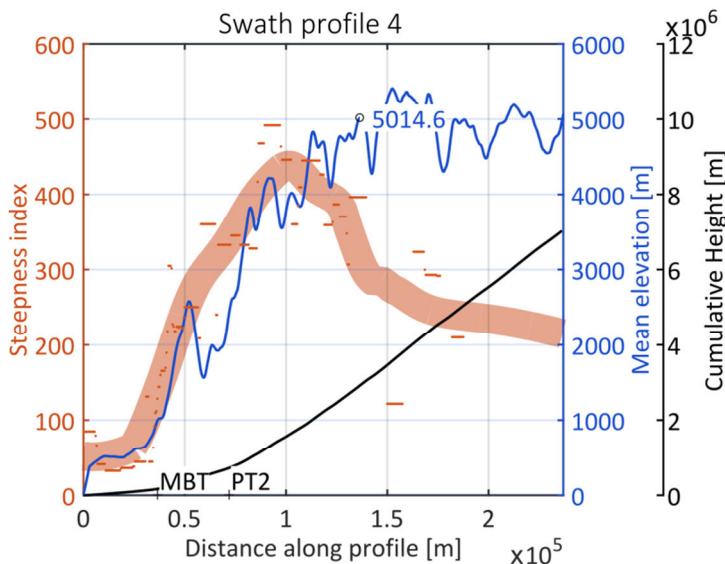


Figure 12. Profile 3

### Profile 3

The increase in elevation in the footwall of the MBT is very rapid (Fig. 12). The elevation increases from 500m to over 3000m within the first 50km north of the MBT. Although this profile does not cross the Kashmir Basin, it appears that the topography follows a similar trend and decreases after a

first local peak. The first peak in this profile is around 3200m in elevation, similar to the previous profile. The maximum  $k_{sn}$  index in the vicinity of the MBT is about 400. However, the smoothed trend of the steepness index clearly shows that the peaks in the steepness distribution along this profile are not as pronounced as in profile 1 and in profile 2. Following this, we observe a drop to less than 2000m in the mean elevation because the swath profile crosses the major valley of the Chenab river and its tributaries. The  $k_{sn}$  indexes decrease simultaneously. The next step in elevation from below 2000 to 3500m approximately coincides with the southern boundary of the Kishtwar Window along strike and is interpreted as the location of the PT2. At this location the Chenab crosses the tectonic window. Thus the elevation decreases again near the stream but it is evident that the channel steepness of the tributaries is much higher than further downstream. Catchments with  $k_{sn}$  values over 500 can also be found in this area. Contrary to profile 1 and profile 2, the second peak in the channel steepness distribution is much higher than the first one. In addition, the absolute  $k_{sn}$  values are much higher than in the previous profiles, which might be related to the deeply incised Chenab valley. Moving further along the profile we can see that the mean elevation of the High Himalaya increases to over 4000m with some peaks higher than 5000m in the swath profile. The elevation at 100km north of the MFT is 4622m. The catchment-averaged steepness indexes scatter but the smoothed trend declines in the same way as seen in profile 1 and 2.



**Figure 14. Profile 4**

#### Profile 4

The fourth swath profile crosses the northwestern expression of the Dhauladhar Range and the Ravi river flowing parallel to the strike of the mountain front in this location (Fig. 13). It is apparent that the distance between the MFT and the MBT continuously decreases from profile 1 to profile 4. The shortest

distance is ca. 35km. In the footwall, the elevation is generally low. The MBT crops out at 1000m above sea level. Thus, not much topography has been build up in the footwall, but it is interesting to observe that the southernmost catchments near the MFT have higher  $k_{sn}$  values than others in the foreland basin. The topography and the distribution of the river steepness in the hangingwall of the MBT differ very much from northeastern patterns. Elevation increases rapidly to the peaks of the Dhauladhar range and gently rise to a mean

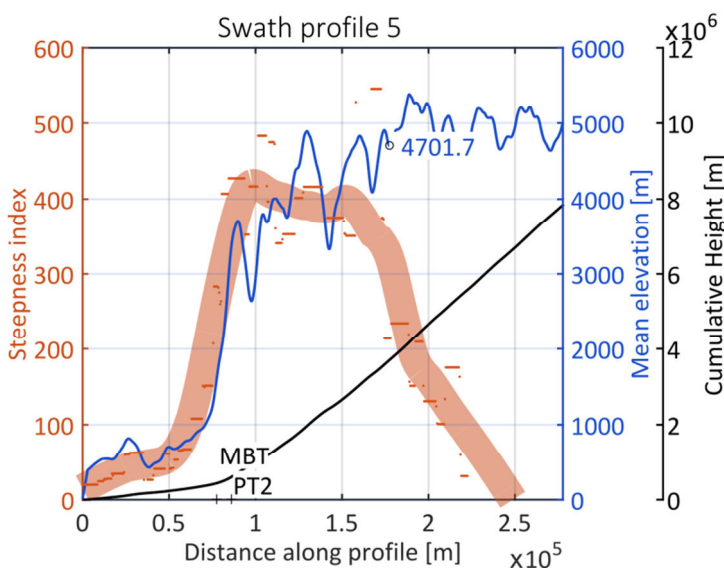


**Figure 13. Profile 5**

elevation of ca. 5000m. This elevation level stays constant in the High Himalaya. The elevation at our point of comparison is 5014m. Looking at the channel steepness we see that the  $k_{sn}$  indexes in the hangingwall of the Main Boundary Thrust steadily increase to a single peak value of nearly 500 and

decrease again moving further along the profile.

#### Profile 5

Similar to profile 4, this profile also crosses the Dhauladhar Range, the Chenab River and the Zanskar Range. It appears that the distance between the MFT and the MBT increases again in

the Kangra reentrant. Furthermore, we see that there are also catchments in the foreland with increased steepness indexes near the Jwalamukhi thrust (Fig. 14). In general, the average elevation slowly increases in the footwall of the MBT but the topography rises rapidly in its hangingwall to up to 3700m. The highest elevations here are above 5000m and 100km northeast of the MBT the elevation is 4701m. The  $k_{sn}$  value in this profile increases to a maximum 546. We can observe that the highest values are located in the hanging wall of the MBT. Moving further away, they decrease again as already seen in the previous profiles.

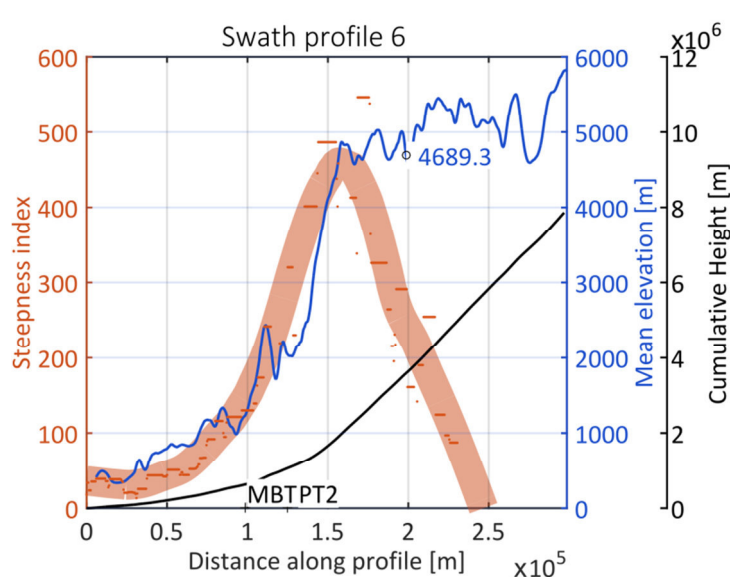


Figure 15. Profile 6

**Profile 6**  
In general, the sixth profile is similar to profiles 4 and 5. The distance between the MFT and the MBT is about 100 km in this profile. The elevation and the steepness of the catchments increase significantly in the hangingwall of the Palampur Thrust and its splays in just some 10 kilometers in the footwall of the MBT (Fig.

15). Few changes can be recognized near the MBT. Major changes in the topography and the river steepness can be seen around the location of the PT2. The change in elevation is very prominent as in profiles 4 and 5. The topography increases with a steep gradient of nearly 125m/km to nearly 5000m, forming a very steep mountain front. Coincidentally, the river steepness rises to values of 547 before they decrease again moving towards the center of the orogen. In contrast to profile 5, the width of elevated channel steepness indexes is narrower.

### Profile 7

This profile describes the topographic setting across the Nahan Salient, a pronounced topographic bulge and the Kullu-Rampur-Window. The foreland is very narrow and topography rises with a high gradient to over 1000m of mean elevation (Fig. 16). Moreover, the steepness of the streams draining the foreland is comparatively high. We do not observe any large increase in elevation in the hangingwall of the MBT, where topography is quite low. The reference elevation at a distance of 100km is 4075m. The High Himalaya becomes more pronounced in the hanging wall of the PT2. In this profile it is interesting to see that the

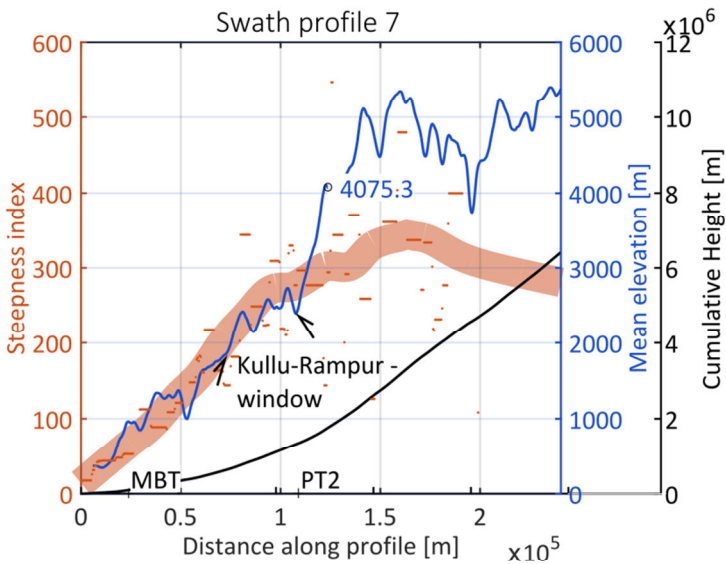


Figure 16. Profile 7

300.

steepness of the catchments uniformly increases from 100 at the MBT to more than 450. The highest  $k_{sn}$  values coincide with an onset of an increase in elevation to the first peaks larger than 5000m. The  $k_{sn}$  indexes decrease moving further into the orogen but they stay relatively high at values ranging between 250 and

### Profile 8 & 9

Profiles 8 and 9 are very close to each other. Thus, they most likely represent the same compressional and structural regime. However, profile 8 mainly comprises the setting around main channel of the Sutlej whereas profile 9 is located further southeast covering the eastern tributaries of the Sutlej (Fig. 9). This arrangement is advantageous because it helps to identify the influence of the large river on the distribution of the steepness indexes. The Subhimalaya is very narrow in both profiles in front of the Nahan Salient (Fig. 17&18). Moving further along the profile we notice a similar increase in elevation in both profiles in the hanging wall of the MBT. Until the onset of the PT2, the trend in the topography, with mean elevations around

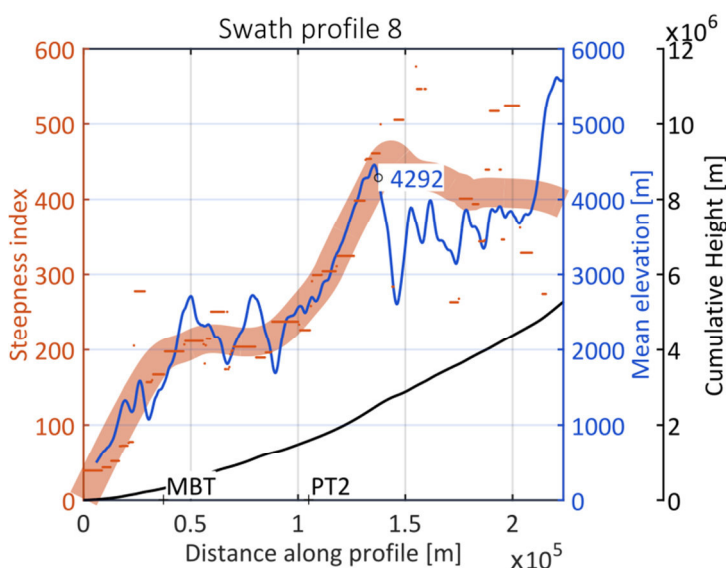


Figure 17. Profile 8

2000m and in the  $k_{sn}$  values remain comparable. The index is constant at ca. 220 in both profiles. It is worth mentioning that we observe similar pattern in the footwall of the PT2 although profile 8 covers High Himalayan klippen, relicts of former thrust nappes in the hanging wall of the MCT (Seeber & Gornitz 1983). In

profile 9 the mean elevation northeast of the PT2 is higher than in profile 8. Nevertheless, the distribution of the steepness indexes is similar. The smoothed trend of the  $k_{sn}$  values ranges between 400 and 500 in both profiles.

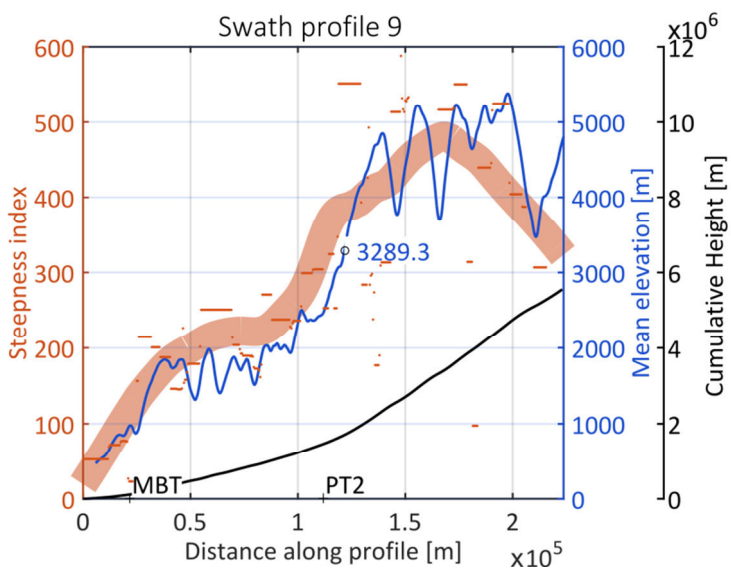


Figure 18. Profile 9

increasing trend in the river steepness from the foreland to the onset of the High Himalaya. Maximum  $k_{sn}$  value is 591, which is also the highest value found in all profiles. The trend declines while moving further along the profile. Due to the low topography in the foreland we see a step in elevation moving into the hangingwall of the MBT. The mean elevation increases to nearly 2000m which is similar to the hangingwall topography in the Nahan Salient. This level can be observed for 50km in the hangingwall of the MBT. In the hangingwall of the PT2,

### Profile 10

A similar pattern to profiles 8 and 9 can be recognized in profile 10, which crosses the Dehra Dun and the Gharwal region (Fig. 19). The distance between the MFT and the MBT is larger here at ca. 30km. The topography and the  $k_{sn}$  values are lower in the foreland compared to the Nahan region. In any case, we also identify a uniformly

increasing trend in the river steepness from the foreland to the onset of the High Himalaya. The High Himalaya rises to mean elevations of ca. 5000m.

### Summary of profile 1-10

The swath profile analysis revealed that some profiles share similar characteristics. Profiles 1 and 2 can be grouped because they share a similar topography with two distinct peaks in the elevation and in the steepness indexes. Furthermore, profiles 4, 5 and

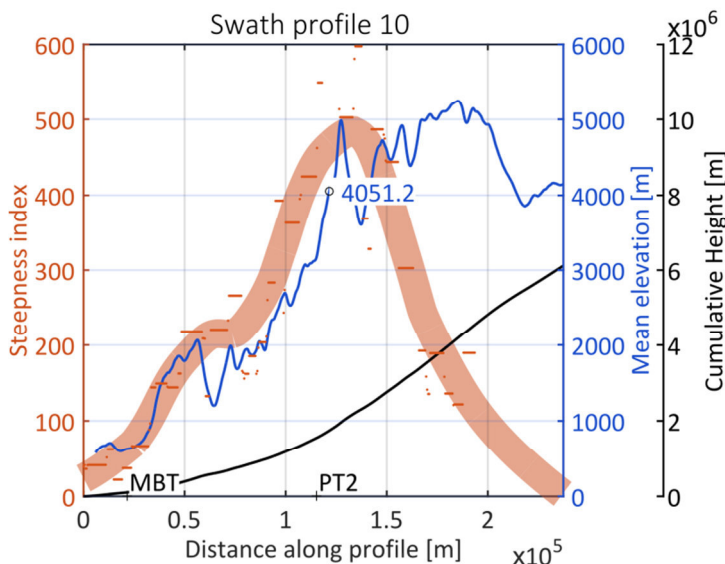


Figure 19. Profile 10

6 can be seen as similar. In these three profiles, the MBT and the PT2 are very closely located. The topography rapidly increases moving across the structural features. Moreover the pattern in the channel steepness is similar. The three profiles show peaks that quickly develop but decline while moving away from the orogenic front. Lastly, we group profiles 8, 9 and 10 together. These profiles share similar cumulative heights. In addition they have a pronounced structural set-up. The distance between the MBT and the PT2 is very similar in all profiles. Profiles 3 and 7 represent the transitions between the three groups. Based on these observations, the profiles can be subdivided in three segments (A1-A3) with similar topographic characteristics.

### The cumulative height

The cumulative height is used as a proxy for the strain that has been accommodated in a specific distance. The results taken from the swath profiles are listed in the following table. Comparing the obtained values with each other it is obvious that the cumulative sum between the MFT and the PT2 is highest in area A3 (profile 1&2) and lowest in area A2 (profile 4-6). By comparing the cumulative height between the MFT and a point 200km northeast of the respective location, we observe a roughly decreasing trend from profile 10 to profile 1 (from 480 km to 327 km).

Prof.	Distance	Cum. height	Cum. height	Cum. height	Cum. height
	between MFT and MBT [m]	Elevation at obs. point [m]	[m] MFT-MBT	[m] MBT-PT2	[m] MFT-PT2
1	74783	3635	544072	1504586	2048658
2	62012	3652	497875	1414915	1912790
3	52685	4622	478866	918170	1397037
4	36473	5014	164615	548013	712628
5	77294	4701	435959	168318	604278
6	98610	4689	620184	420867	1041052
7	41056	4075	93702	1256703	1350406
8	21677	4292	310592	1273166	1583759
9	21578	3289	111863	1344641	1456505
10	37395	4051	102962	1441085	1544047
					4807484

## Description of fault-parallel swath profiles

### MBT-profiles

In order to determine the role of the MBT and to detect along strike fault displacement variations, we created two swath profiles parallel to the strike of the thrust fault, one in the hangingwall north of the MBT and one in the foot wall (Fig. 8). In the following figure, we see the mean steepness index of the catchments in the hangingwall and in the footwall plotted against the distance along the fault (Fig. 20). Smoothed fitting curves visualize the main trend along the fault. The relation between catchments in the hangingwall to those in the footwall is shown in the lower plot as the difference in steepness indexes. The 0 km tick in both plots is northwest of the Kashmir Basin.

Here, we recognize that the channel steepness indexes in the footwall are generally lower than in the hangingwall. However, both profiles show distinct, along-strike variations. According to the hangingwall of the MBT, we observe that the steepness indexes oscillate between 300 and 200 from the starting point to kilometer 450. Following the profile, we see a drop from 300 to almost 100 between kilometers 450 to 500. Interestingly, the oscillating pattern continues moving further along the profile but the values fall in the range between 100 and 200. Looking at the catchments located in the footwall of the MBT, one can point out that the steepness index in the northwest is nearly as high as in the hangingwall. However, the

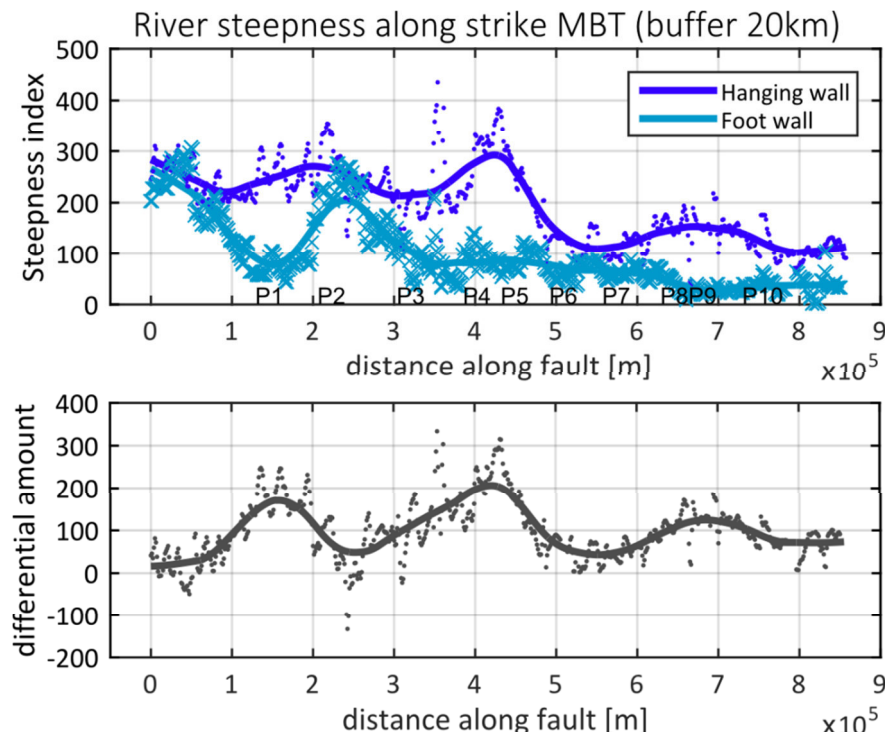


Figure 20. Along-strike profile of the MBT. The upper subplot shows the along strike variations of catchment's steepness indexes in the foot and in the hanging wall of the MBT. The lower subplot visualizes the difference at each point along the fault.

channels ( $k_{sn}=250$ ) become gentler ( $k_{sn}=100$ ) moving from kilometer 0 to kilometer 150. In the following 200km, the steepness index increases to more than 200 and decreases again to values ranging around 80 near the location of profile 3. This level remains relatively constant until kilometer 650. Here, we see a small drop in the channel steepness from  $k_{sn} \approx 80$  to  $k_{sn} \approx 50$ .

Regarding the lower plot showing the difference in the channel steepness, we see that there is almost none in the northwestern part of the study area (Fig. 20). However, we observe an increasing trend in the profile between kilometer 80 and kilometer 150. The maximal difference in channel steepness at this point is nearly 200. This location coincides with the local minimum in the footwall. Moving further, the differential amount decreases until kilometer 250. Here, the difference is ca. 50. Following this, we see another increasing trend to a difference of 200 in the  $k_{sn}$ -indexes. This maximum value is at kilometer 450 coinciding with the location of the maximum steepness indexes in the hanging wall. The trend declines in the following section but increases again between kilometers 550 and 700. In general, this second plot shows an oscillating pattern with 3 maxima along the whole profile.

### PT2-Profiles

In this profile, we recognize again that the channel steepness in the footwall is generally lower than in the hanging wall (Fig. 21). We split the hanging wall profile into three sections. The northwestern section from kilometer 0 to kilometer 150 is described by one increasing and one decreasing trend falling in the range between 150 and 270. The total value increases in the following section (kilometer 200 to 550) above 300. In addition, the smoothed trend shows low oscillation. In the third section (kilometer 550 to 750) we see again an increase in the total steepness to values above 350. Thus, the general northwest to southeast trend is increasing.

The channel steepness in the footwall-catchments is also lowest in the northwest. Again we can subdivide the profile into three different sections. The first one showing values around 100 can be identified between kilometer 0 and 150. This is the same range as in the profile of the hanging wall of PT2. Here, the smoothed trend ranges between 200 and 300. This second subdivision is evident from kilometer 150 to kilometer 350. In the last part we see a relatively constant trend around 200 with only few outliers. In general, we see less, along-strike variations in the channel steepness compared to the MBT profiles.

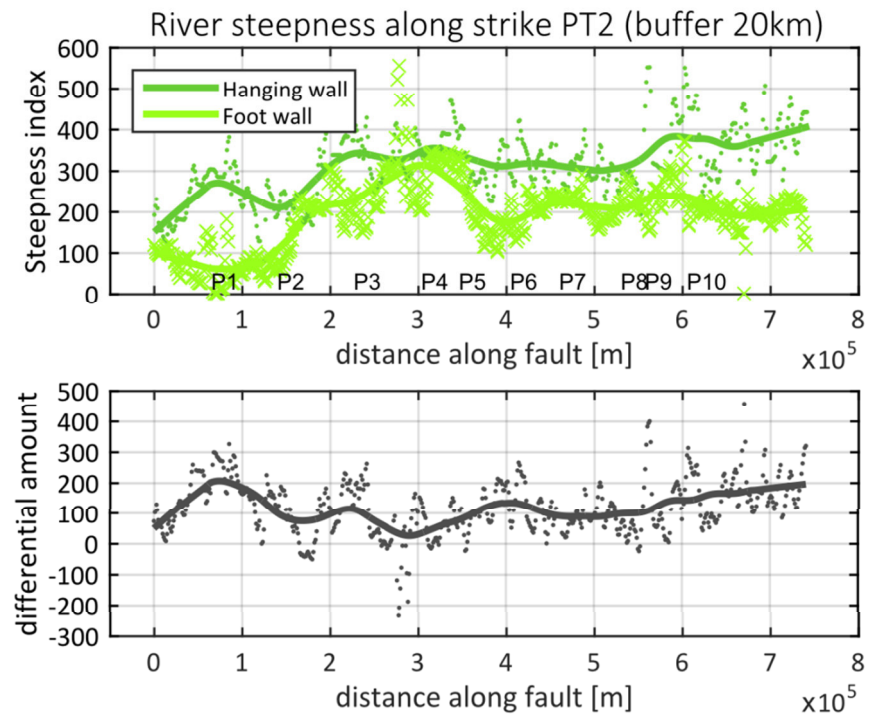


**Figure 21. Along-strike profile of the PT2. The upper subplot shows the along strike variations of catchment's steepness indexes in the foot and in the hanging wall of the PT2. The lower subplot visualizes the difference at each point along the physiographic transition (PT2).**

The second subplot is more diverse than the plot for the MBT (Fig. 21). Here, a discrete oscillation cannot be assigned to the PT2. However, we observe a first subdivision between kilometer 0 and kilometer 150 with a local maximum at kilometer 85. The peak difference in channel steepness is around 300. Between kilometers 150 and 550 the smoothed trend ranges between ~60 and ~160. The southeastern part of the profile shows an increase in the differential amount between footwall and hanging wall catchments. The channel steepness values increase to around 200 at the very end of the profile.

## Discussion

### Significance in data distribution

As described by the topographic analysis above the northwest Himalaya can be subdivided into three segments, here named A1, A2 and A3. In order to prove local strike variations in the topographic characteristics for significance in their distribution we have performed a hot-spot-analysis (Fig. 22). For Area A1 and A2, the cluster shows a significant concentration of steep catchments located in the hanging wall of the PT2 (Fig. 22). It is worth mentioning, that the hotspot also includes the Dhauladhar Range and the Kishtwar window. The observation of this hotspot supports the assumption that the PT2 can also be assigned to systematic changes in

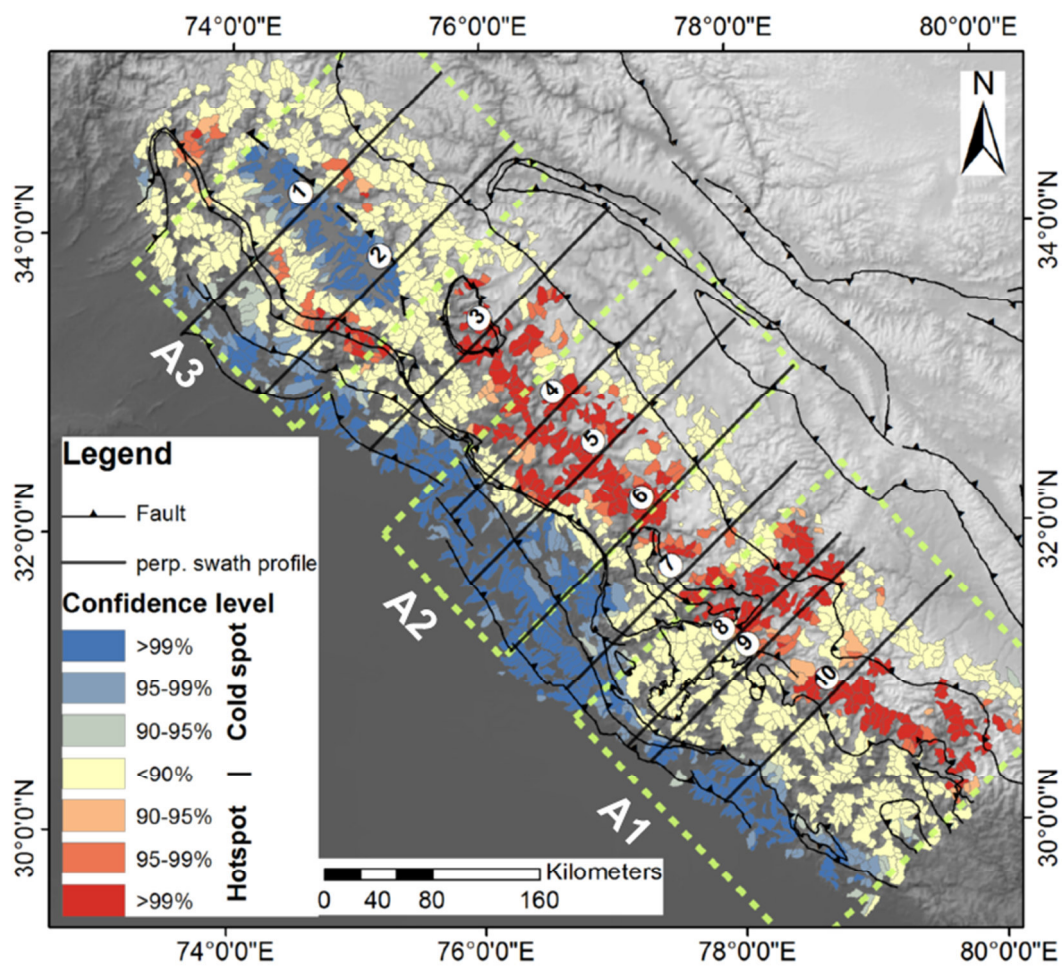


**Figure 22. Hot Spot Analysis.** Statistically significant areas of high erosion are colored with shades of red. Regions with low erosion rates are blue. A confidence level lower than 90% either results from intermediate steepness indexes or a non-significant amount of high or low indexes around. Hot Spot areas can be found around the PT2 moving from area A1 to the Kishtwar Window, the Dhauladhar range and at the southern and the northern boundary of the Kashmir Basin. Cold spots are to be found in the vicinity of the Kashmir Basin and in the Subhimalaya except in the hanging wall of the MWT.

topographic characteristics, which will be discussed further below. Furthermore we identify the Subhimalaya as a cold spot. However, this observation is probably biased by the lithologic contrast, as in general within the Subhimalaya only partly consolidated or un-consolidated

lithologies are exposed. Due to the fact that the cluster analysis includes all catchments inside the study area, the rivers draining the weaker substrate of the Subhimalaya automatically become a cold spot. In Area A1, it appears that the catchments between the MBT and the PT2 can be assigned to intermediate values. This well-defined band between the PT1 and the PT2 narrows toward the northwest. In Area A2 and especially at the foot of Dhauladhar Range, it is not present anymore. Here, we see a rapid change from a cold to a hot spot. We interpret this as a superposition of the PT1 and the PT2 and might be related to recent fault activity along the toe of the Dhauladhar Range. In Area A3 it is worth to point out that there are hotspots in the front but also in the back of the Kashmir Basin, indicating tectonic activity at several locations. However, we see that the distribution of steep channels is not significant for the whole length of the two ranges, neither for the Pir Panjal Range nor for the Greater Himalayan Range. For the Pir Panjal Range, bounding the Kashmir Basin to the southwest, the hotspot is located in the south between the Chenab and the Poonch River, as recognized in Profile 2 crossing this location. According to the northeastern boundary of the Kashmir Basin, the Greater Himalayan Range, we identify a small hot spot around the location of profile 1. Indeed, the swath profile analysis shows congruent results. Profile 2 presents a higher steepness index at the first front than profile 1 and vice versa. These observations are supported by the cluster analysis and are proved to be not random. In addition, we identify a cold spot in the vicinity of the Kashmir Basin. The cold spot in the Subhimalaya is very small and bounded by the MFT and the Medlicott-Wadia Thrust (MWT). The catchments in the hanging wall of the MFT cannot be assigned to a confidence level of more than 90%. Thus their steepness indexes are not as low as in the rest of the Subhimalaya which indicates that the region in the hanging wall of this thrust experiences an exceptionally high amount of erosion compared to other regions in the Subhimalaya. I relate this to recent thrusting along the frontal faults.

## Applicability of the method

The most striking advantage of the method is that we can investigate the distribution of a parameter approximating the erosion rate in 2D on a sub-orogenic scale. Considering topographic steady state, assuming that the southern part of the mountain front deforms in a brittle manner and that the concept of a critical orogenic wedge (Davis & Dahlen, 1983), which has been applied to southern parts of the Himalayan wedge before, as well as approximate uniform conditions in the erosive process along strike exists, we can transpose this proxy for erosion to rock uplift and thus to tectonic activity. Unfortunately, our approach presumes that the parameters describing the erosive process ( $K$ ,  $n$  in Eq.1) and the drainage basin hydrology ( $m$  in Eq. 1) are constant for the whole study area. Indeed, it has been shown that the  $m/n$

ratio falls in a restricted range and that its influence on the channel gradient is relatively low (Whipple & Tucker 1999). The effective erosion coefficient K which includes the weathering resistivity, the channel width and the channel morphology has a larger impact on the magnitude of the channel steepness and the river's response time to tectonic and climatic changes. According to these terms four main issues arise for the application of a large scale river steepness analysis with fixed parameters. These four points are the differences in the erosive resistivity between the lithologic units, the precipitation gradient, the presence of glaciated areas and the differentiation between alluvial and bedrock draining rivers.

One of the main characteristics within the Himalaya is that different physiographic units mainly consists of respectively, similar lithologies along strike (Hodges 2000). Thus, along strike variations are expected to be limited and therefore negligible for most of my analysis. Furthermore, precipitation data show a very pronounced orogen-perpendicular change in the distribution of the rainfall but along strike changes are rather exceptional (Bookhagen & Burbank 2006). Thus, I assign along strike changes in the channel steepness solely to changes in the rock-uplift and not to changes in the effective erosion coefficient (K). Another completely different issue derives from the erosive agent. Parts of the study area are glaciated or covered by moraine sediments. Studies have shown that channels in glaciated areas differently respond than those of fluvial basins, as glacial erosion processes act very different and disturb the fluvial characteristics significantly (Brocklehurst & Whipple 2007; Hoffmann et al. 2013). Especially in areas with rapid rock uplift where fluvial rivers tend to steepen, glaciated landscapes steepen just little (Brocklehurst & Whipple 2007). In order to avoid misinterpretations based on this term I excluded areas where I identified glacial morphology from the dataset. According to the last issue, it has been shown that the type of the underlying substrate is crucial for the rate of incision. Alluvial rivers usually incise faster into the underlying substrate than bedrock rivers. However, the differentiation between alluvial and bedrock rivers from satellite images is complicated and inaccurate. In order to solve this lack of information it requires detailed field observations which are not suitable size of the investigated area. However, we assume that alluvial rivers are mainly only present in parts of the Subhimalaya and the Kashmir Basin and rarely occur in the rest of the study area. Earlier studies have documented that most rivers in the Lesser and High Himalaya are bedrock rivers, where sediment covering the base of the river channel is moved during high runoff levels and annual floods during major rainfall events in the monsoon season (Wulf et al. 2010).

With respect to these terms we think to use a good tool that produces a trustworthy output approximating the 1<sup>st</sup> order distribution of catchment-wide erosion rate in the NW Himalaya.

## **Active out-of-sequence thrusting vs. elastic behavior of the upper plate**

In the central Himalaya, Ader et al. 2012, claim that the interseismic deformation in the upper plate of the Central Himalaya is purely elastic and that the accumulated strain is released by large magnitude earthquakes along the MHT without any significant shortening of the hanging wall. They claim that the background seismicity is not sufficient enough to release the build up interseismic stress. Moreover they see it as an indicator for areas of rapid stress increase. Thus, they appeal that the behavior of the upper plate is mainly elastic (Ader et al. 2012).

Such analysis is not available for our study area. We cannot exclude the occurrence of large earthquakes with long re-occurrence times rupturing the whole MHT but we assume that the recorded seismic activity is at least an indicator for the elasto-plastic behavior of the hangingwall. This explanation is more sufficient in order to explain the prominence of the Greater Himalaya which is present for millions of years and the concurrent high steepness indexes at the range front. However, we examine the erosion pattern and the related tectonic mechanisms for each characteristic area, respectively.

## Area A1 - A Central Himalayan analogue

We grouped the profiles 8, 9 and 10 because they share similar topographic characteristics into segment A1 (Fig. 23). The distance between the MFT and the MBT amounts in all profiles ca. 20-30 km. Although the critical taper wedge models are different for the Nahan Salient and the Dehra Dun Reentrant (Singh et al. 2012), we have indications for a similar structural

setting in the remaining part along the profiles. In all three profiles, it is noticeable that the area between the MBT and the PT2 has a relatively low relief. Along the profiles, this

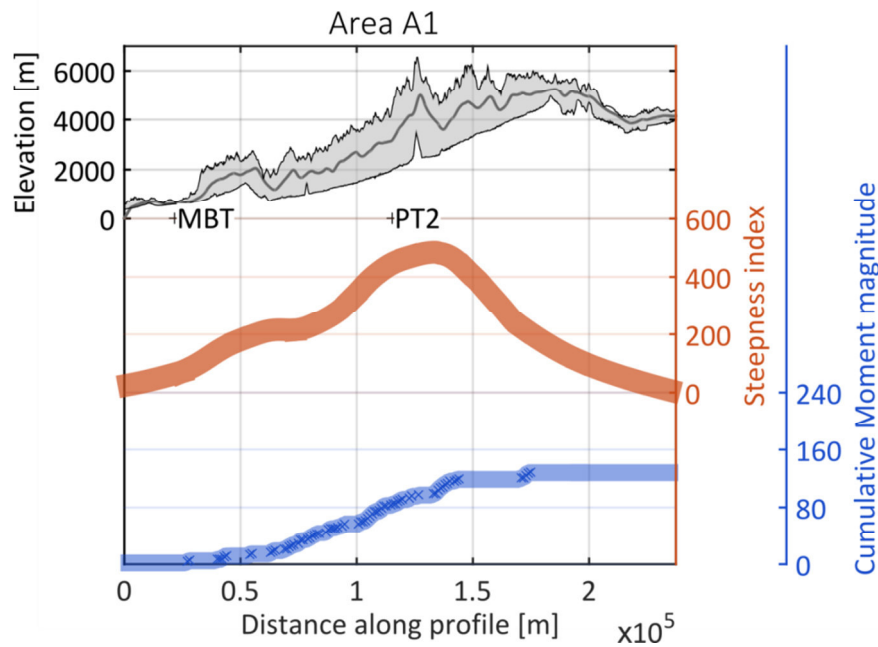


**Figure 23.** Representative swath profile for area A1 including the elevation pattern and the steepness index distribution (swath width 20km) and the cumulative sum of moment magnitudes of seismic events (swath width 100km) from 1999 to 2011, (Mahesh et al. 2013)

means that the trend is evident for 75-100km.

Even Profile 8 which mainly covers High Himalayan Crystalline shows this pattern. We cannot identify any major changes in elevation which can be correlated to the MCT. This observation supports previous assumptions about inactivity of the MCT (Seeber & Gornitz 1983). In addition, it is remarkable that the smoothed trend of the steepness indexes for the Lesser Himalaya (ca. 210) is similar in the profiles 8-10. This implies that the erosion rate for each catchment in area A1 between the MBT and the PT2 is approximately similar. Similarly, we also observe a rapid increase in the elevation and the steepness indexes at the PT2 in all three profiles. These results are interpreted to display areas of increased erosion. In addition, these results agree in terms of the spatial distribution of exhumation rates which are highest in the northern Kishtwar window (Thiede et al. 2009). Nevertheless the method is inappropriate to decipher the fault geometries in the subsurface. A seismic survey in the Garwhal region promotes the idea of a flat beneath the Lesser Himalaya and a duplex structure beneath the PT2 (Caldwell et al. 2013), which is related to a flat-ramp-flat structure within the MHT beneath. However, the lack of highly resolved seismic profiles has so far prevented the recognition of these duplex structures. Its presence is mainly based on the interpretation of

balanced cross sections in several segments along strike of the Himalaya e.g. (Robinson et al. 2003). In order to determine the mechanism responsible for the enhanced erosion around at the PT2 we include a record of seismic events. It is obvious that the seismic activity is pronounced in the vicinity of the PT2, very similar as observed in Central Nepal (Pandey et al. 1995). Previous studies assume that local seismicity occurs mainly at a ramp and that the frontal part of the MHT is locked (Avouac & Cattin 2000). The motion at the MHT beneath the Greater Himalaya is probably best described by aseismic creep. Thus, it has been proposed that the location of the events strongly depends on the geometry of the ramp and/or the duplex structure or a splay fault in the subsurface. Because of the seismic activity and the occurrence of steepened river channels, we expect a similar accommodation of shortening or at least an out-of-sequence activity of faults for area A1 as described in model B or C. A respective scheme illustrating the geometry in the subsurface in A1 can be seen in figure 24. In general, we found the Himalayan deformation and the topographic evolution of the segment A1 similar to models proposed for central Nepal.

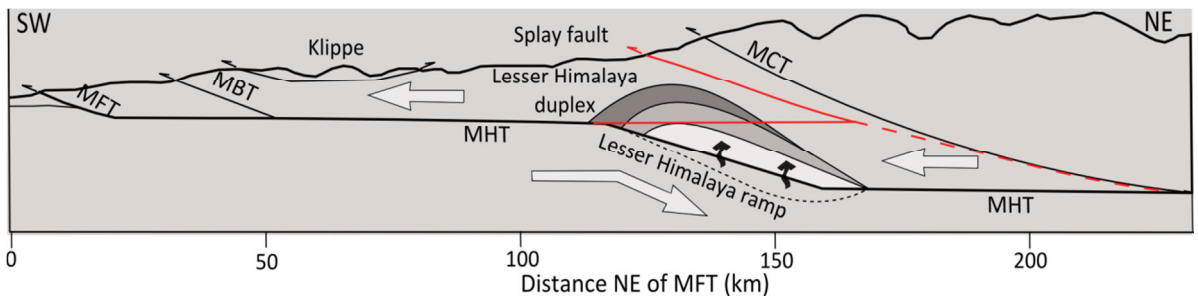


**Figure 24.** Conceptual scheme for the subsurface geometry of faults in area A1; comparable to the classical setting in the Central Himalaya. The duplex structure (grey shades) is favored by many previous studies. However, its presence is highly debated (Elliot et al., 2016) (Whipple et al., 2016). Alternative models favor out-of-sequence thrusting at splay faults (red line) and not the presence of a ramp or a duplex structure (Whipple et al., 2016).

## Area A2 – The Chamba Himalaya

Seeber & Gornitz (1983) pointed out that only in the Kashmir Himalaya where the MBT, the MCT and the MFT are close to each other, steep river gradients can be associated to the activity of the MBT. This might be true for large rivers but the analysis of tributary catchments

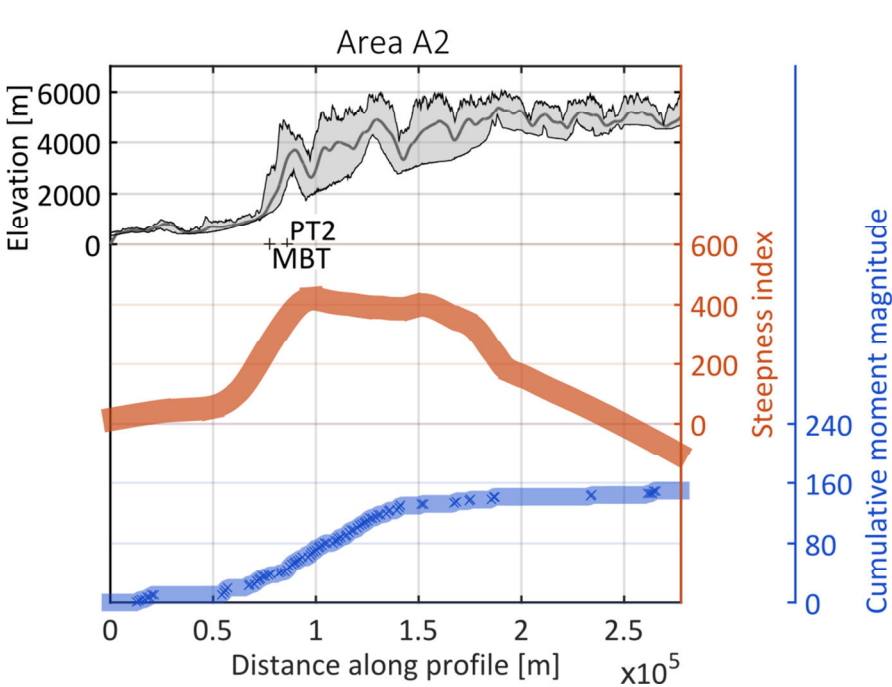
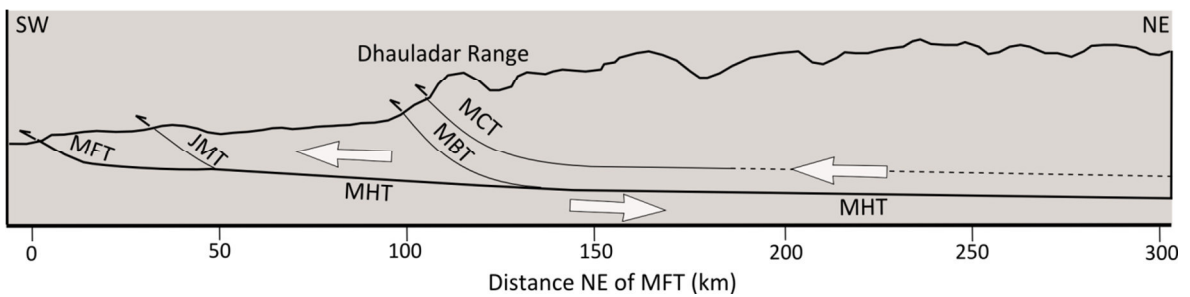


Figure 25. Representative swath profile for area A2 including the elevation pattern and the steepness index distribution (swath width 20km) and the cumulative sum of moment magnitudes of seismic events (swath width 100km) from 1999 to 2011, (Mahesh et al. 2013)

smaller than 250km<sup>2</sup> reveals that this is also true for the northern part of the Kangra Reentrant. Here, we observe an immediate, large increase in the elevation and in the steepness index in the hanging wall of the MBT

at the Dhauladhar Range (Fig. 25). The MBT and the MCT are closely stacked implying that the PT1 and the PT2 are in a superposition. Apatite fission track and Zircon(U-Th)/He cooling ages imply that the structural architecture of the Chamba Himalaya is best described by a flat basal detachment below the Pir Panjal Range and the Gianbul Dome and a steep ramp responsible for the uplift of the Dhauladhar Range (Deeken et al. 2011). Furthermore, the data from the same study showed that exhumation in this part of the Himalaya is locally increased at the Dhauladhar Range for the past 10 Ma (Deeken et al. 2011). Our results are in good agreement with the prediction of the low temperature chronology studies that erosion is highest at the front of the Dhauladhar Range. The accommodation of shortening at the MBT is also supported by GPS velocities which are much higher in the hanging wall than in the footwall. By comparing the cumulative magnitude profiles from A1 and A2 it is obvious that in A1 the seismic events also occur southeast of the PT2. In A2 we see that epicenters are sharply bordered by the MBT. (The Dhauladhar Range is not running perfectly perpendicular to the profiles. Therefore and due to triangular reason, some events in the profile are drawn in the footwall of the MBT, which is actually not the case.) Unfortunately, we do not have

information about the depth of the events, or they are poorly constraint but we assume that they mainly contribute to slip along the subhorizontal MHT as we assume that the ramp of the MBT fault plane is interseismically locked. The recent activity and thus the out-of sequence thrusting at the MBT were a plausible explanation for the observed steepness indexes at the southern range front (Fig. 26). However, similar to area A1, we cannot rule out that rare, large events at the MHT rupture a fault in the foreland-fault and -thrust-belt. This is assumed to have happened in 1905 during the Kangra-earthquake which is believed to have ruptured the Jwalamukhi thrust.



**Figure 26. Simplified profile across the Chamba Himalaya; mainly inferred from gained data and geologic maps (Hodges, 2000).**

### Area A3 – The Kashmir Himalaya

Previous studies suggest that the intramontane Kashmir Basin developed around 4-5 Ma ago due to the translocation of the active faultzones towards the southwest, and thereby established a new mountain front (Burbank 1983). The MBT which was active by that time have uplifted the Pir Panjal Range and build the new southwestern topographic boundary of the Kashmir Basin. The active mountain front propagated further when the Medlicott-Wadia-Thrust and the Suruin-Mastgarth Anticline developed, most likely since 2Ma ago (Burbank et al. 1986). For further interpretation of our results we adopt the structural profile from Burbank et al. in this study, as high level agreement between his assessments and our results (Fig. 28). Hence, we can add that today, two distinct peaks in the steepness indexes indicate that the Pir Panjal Range to the south as well as the Great Himalayan Range to the north of the Kashmir Basin experience increased erosion (Fig. 27). We observe that the maximum channel steepness indexes in the Kashmir Himalaya are in total lower than in area A1 and area A2 which is counterintuitive, if we relate it to the precipitation rate, as this decreases from east to west at the Himalayan front (Bookhagen & Burbank 2006). We rather favor to interpret our proxy for the erosion rate in the following way:

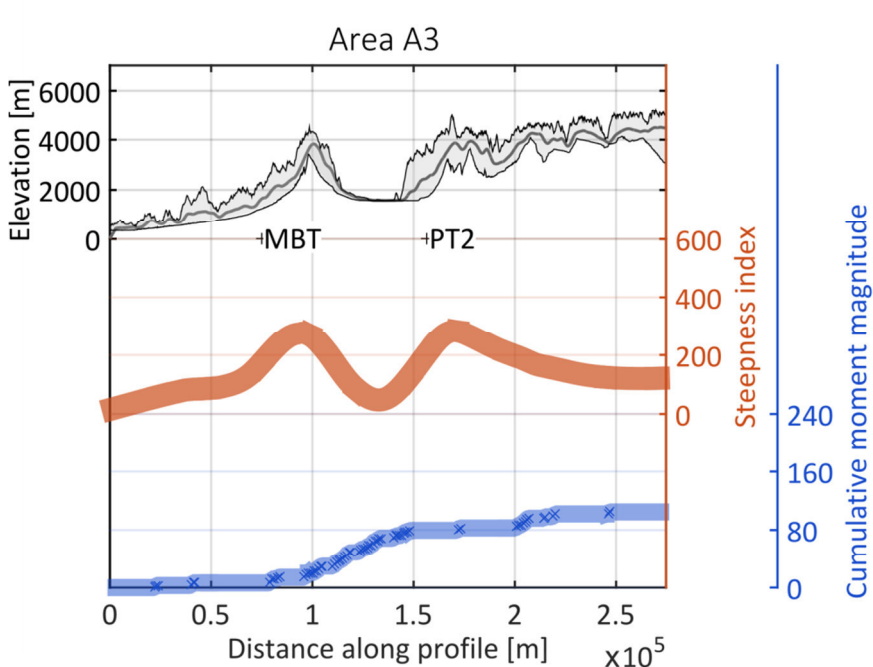


**Figure 27.** Representative swath profile for area A1 including the elevation pattern and the steepness index distribution (swath width 20km) and the cumulative sum of moment magnitudes of seismic events (swath width 100km) from 1999 to 2011, (Mahesh et al. 2013)

A decrease in the convergence rate, due to the north bend of the Himalayan arc along the northwestern syntaxes of the Himalaya, could result in a lower uplift rate. However, with a

conservative view, this does still not explain

why the channels in the Pir Panjal Range are as steep as those in the Greater Himalayan Range. Therefore we additionally assume that the strain and the crustal shortening is accommodated along multiple faults uplifting both range fronts.

Unfortunately, the present day record of microseismicity to help verify this is not sufficient enough, which relates to the fact that these faults are at present seismically locked. We see that most of the events are located southeast of the Great Himalayan range, but the density is very low and not sufficient enough for respective statements. However, from profile 1 and 2 we clearly see that the erosion is not equal along the two ranges. The data distribution in Profile 1 shows lower steepness indexes at the frontal peak compared to profile 2. In addition,

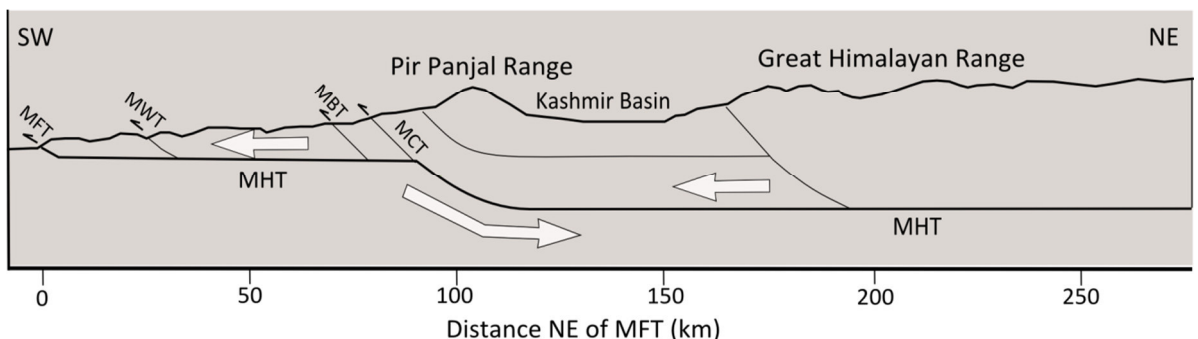


**Figure 28.** Simplified profile across the Kashmir Himalaya. adopted and modified from Burbank, et al., 1983

we observe higher values in the second peak of the Great Himalayan range in Profile 1. Therefore these observations are not conclusive but in order to interpret the along-fault changes in the erosion we prefer to use the respective profiles.

## Along strike variations

### Recent denudation at the PT2

The analysis of the perpendicular profiles and the thermochronologic studies already revealed that the long-term denudation of the Himalaya is pronounced in the vicinity of the PT2. However, the along strike profile shows that the erosion rate along the PT2 in the northwestern Himalaya is not uniform along strike. Moreover, it presents that the contribution of the respective uplifting structure is also not uniform along strike (Fig. 29). In area A1, the difference in the steepness indexes supports the assumption that the structure accommodates a large amount of shortening resulting in the uplift of the Greater Himalaya. Analogues of this setting can also be found in other parts of the Himalaya, such as central Himalaya (Lavé & Avouac 2001; Herman et al. 2010). But here, we observe that the trend in the rate of the activity of the uplifting structure decreases towards Area A2. The local minimum between A1 and A2 is located around the Kullu-Rampur window, which implies that here the contribution of the out-of sequence activity is slightly lower compared to Area A1. Never the less the erosion rate in total is comparable. This observation is supported by AFT ages from the literature (Thiede et al. 2009)

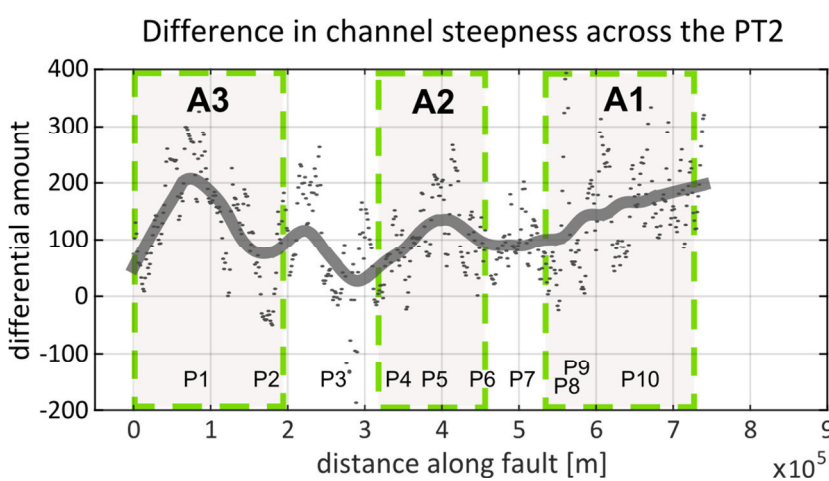


**Figure 29.** The relative tectonic activity of the PT2-underlying structure is not uniform along the transition zone. Peaks in the graph suggest active, out-of-sequence segments. Moreover, we observe increased values in all three areas.

In A2, we observe a different setting. The morphometric analysis revealed that the PT2 can be extended towards the Dhauladhar Range. But we think that the architecture in the subsurface changes from A1 and A2. We assume that the

transition in A2 is caused by the tectonic activity with a deep-seated MBT-fault ramp within this segment and not by a duplex structure or shallow splay faults in the subsurface (for better visualization see figure 26.). The following local maximum in the profile is worth to mention because it can be sharply assigned to the area of the Kishtwar window. The averaged trend is comparable to the values of the Kullu-Rampur Window but the single catchment's values are clearly higher in the Kishtwar-Window. Therefore, we assume that at the Kishtwar window

experiences more rapid exhumation than the Kullu-Rampur-Window. But this assumption is not supported by long term exhumation rates based on AFT-ages (Thiede & Ehlers 2013).

Insertion: The pronounced exhumation and denudation of the units at the Kishtwar window could indirectly lead to the steepening of the Chenab tributaries which have to adjust to the more rapid incision of the main river channel. This hypothesis would partially explain the increased catchment steepness of the tributaries of the Chenab north of the Dhauladhar Range. Another explanation would be that the recent rivers still have not been adjusted to the channels which had been deeply incised by glaciers during the last glacial maximum (Eugster et al. 2016).

According to the Kashmir Himalaya, the PT2 profiles support the first assumption that the tectonic activity of the northern Greater Himalayan range is not uniform. Although we observe a decrease in the total channel steepness, the northwestern part of the range probably experiences more erosion. We see a definite maximum in the difference in channel steepness around profile1, which implies that the structure beneath the PT2 is tectonically active and uplifting the Greater Himalaya. In this specific case and based on the geologic history of the Kashmir Basin, we think that it is most likely that the former MBT is responsible for the uplift.

In general and taking into account that the used method is an average proxy for the erosion over multiple thousands of years, we assume that the activity of the structural features responsible for the PT2 is not spatially uniform along strike.

### Tectonic activity of MBT-Segments

The steepness indexes in the hanging wall of the MBT are much higher in the western part of the profile (Fig. 20). However the proclaimed out-of-sequence activity of the MBT is not continuous. This is well displayed in the along strike profile (Fig. 30). In A1 one can discuss about a slightly enhanced activity of the MBT in the Nahan Salient but the difference to fault segments at the Dehra Dun is quite low. However, within the Dehra Dun re-entrant Quaternary faulting has been proposed (Whittaker 2012). It is more interesting that the trend decreases between the two characteristic settings of A1 and A2. This local minimum will be discussed in combination with the minimum between A2 and A3.

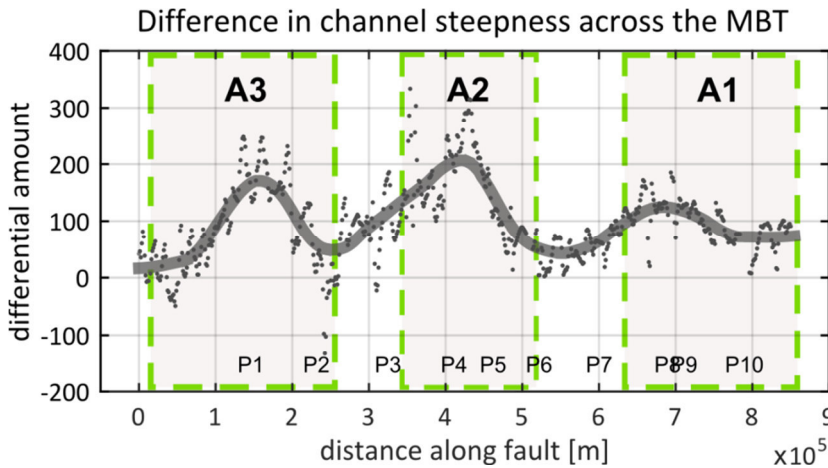


**Figure 30.** The relative tectonic activity of the MBT is also not uniform along strike. The oscillating pattern in the graph suggests active fault segments in all three areas.

According to the tectonic setting in A2 and as already mentioned, we expect that out-of-sequence thrusting at the MBT is responsible for the uplift of the Dhauladhar Range. This is well illustrated in the along strike profile which shows the

highest difference in the steepness index at this location of the mountain range. Between A2 and A3 we see another minimum which is located east of the outlet of the Chenab. Interestingly, this location is coincident with the local maximum in the PT2 profile when we look perpendicular to the orogenic strike (or along profile 3). Therefore we argue that here the located MBT fault segment is inactive and the remaining strain is at least partially accommodated at the respective PT2-forming structure in the hinterland. Vice versa, the MBT-segment west of the Chenab outlet shows indications for an increased tectonic activity. The pendant at the PT2 shows a local minimum in the activity. These two observations are crucial because they imply that stress is not solely released at the frontal thrusts or at the MBT but also at fault segments below the Greater Himalayan Range. Furthermore and unlike the profile of the PT2, the areas with relatively increased erosion in the hangingwall are more pronounced. The observed pattern reminds on an oscillating wave function. This is very interesting because one could use a specific wavelength for the description of the activity of the MBT. But at this moment we are satisfied with the identification of the active segments.

## Total strain distribution

Regarding the along strike profiles, we observe a decrease in steepness indexes along the PT2 from the northwest to the southeast. Although it is speculative, a decrease in erosion can be an indicator for the decrease of the arc-normal convergence rate towards the northwest (Banerjee 2002). In contrast to a steady decrease, it seems that the activity of the MBT and the faults in the Subhimalaya describe a contrary curse. In contrast to the PT2 we see an increase in the steepness index from southeast to northwest. Similarities can be seen in a

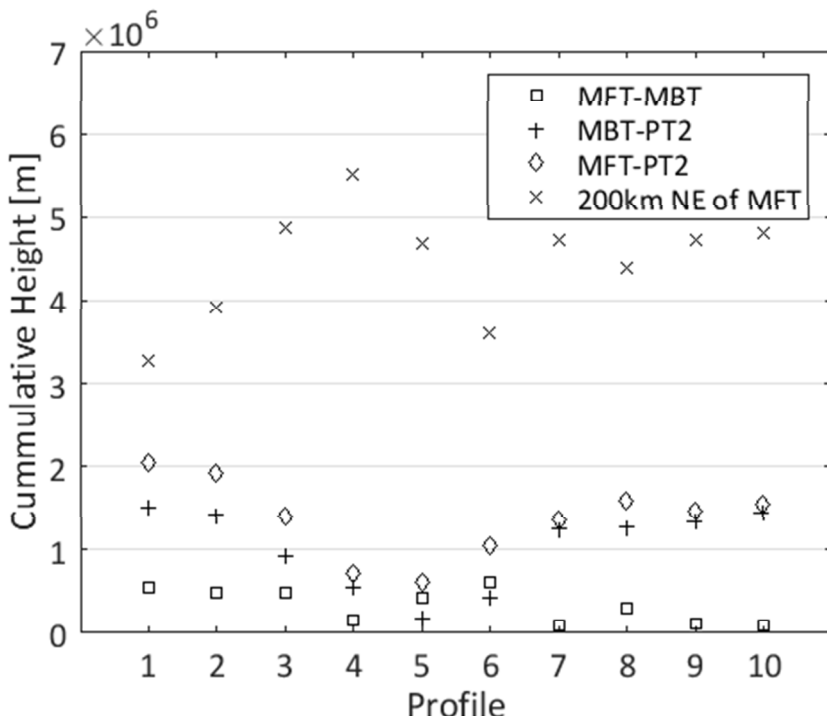


**Figure 31.** Cumulative heights from the perpendicular profiles 1-10. The cumulative height serves as a proxy for the total amount of strain that has been accommodated in the topography. Here we display the lateral variation between four intervals.

figure that displays the distribution of the cumulative height (Fig. 31). The cum. height calculated for a the distance between the MFT and a point 200km northeast of the PT2 describes a roughly decreasing trend moving towards the northwest. We know that the Monsoon activity decreases towards the northwest (Bookhagen & Burbank 2006), thus we would rather expect an increasing amount of topography in this direction because the erosion rate is assumed to sink. This counterintuitive observation can be explained by different processes but the decreasing convergence rate between India and Eurasia is probably the best explanation for the decrease in the cumulative height.

Nevertheless the figure also shows that the PT2-structure is not decoupled from the activity of the MBT. The accumulated strain between the MFT and the MBT (or the PT2) is high in the profiles 1-3 and 7-10. The activity of the PT2-structure annihilates this pattern which can be

seen in the distribution of cumulative sums 200km northwest of the transition zone. This accounts for a strong relation between the both structures.

## Relationship to published rates

Considering Eurasia as stable the Indian craton moves at a rate of  $37\pm1\text{mm/yr}$  towards NNE (Wang et al. 2001) (Molnar & Stock 2009). Previous studies proposed that most of this convergence is accommodated via slip on the MHT (Lavé & Avouac 2000). For the Central Himalaya, the MHT absorbs about 20mm/yr which is about half of the total convergence rate between India and Eurasia (Lavé & Avouac 2000). Here, it is expected that the convergence is

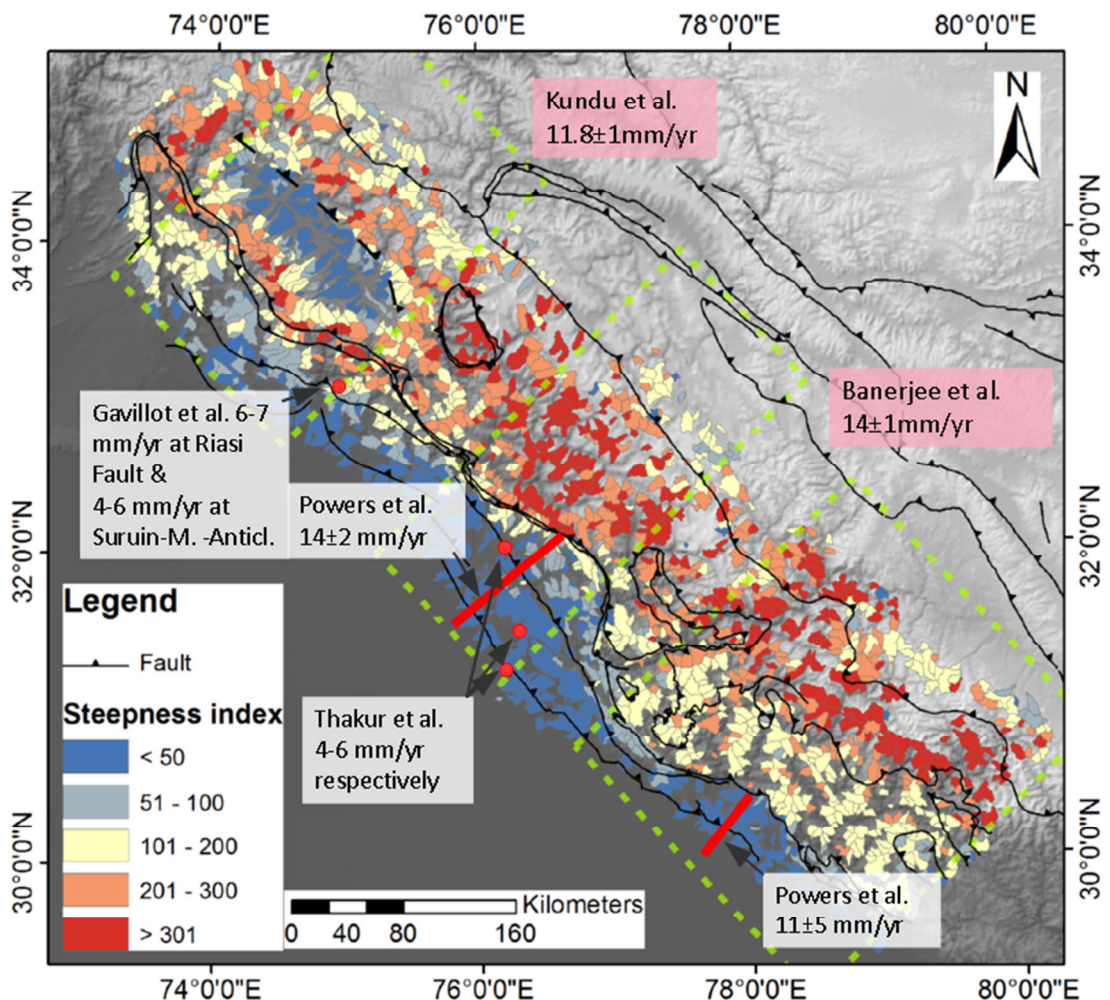


**Figure 32.** Steepness index map including published shortening rates from the study area. The dashed black line in the Kashmir Himalaya, shows the expected location of an out-of sequence thrust. Red dots: point measurements; Red line: balanced cross sections; Rose textboxes: rates from GPS measurements.

purely arc-perpendicular (Silver, Calvin R. P. et al. 2015), (Ader et al. 2012). Due to the arc-shape geometry of the Himalaya, the western part of the orogen is more oblique to the sense of the plate motion. Thus the compressional regime in the northwestern Himalaya is described by an oblique convergence resulting in strain partitioning (Silver, Calvin R. P. et al. 2015). For Area A1 and A2, geodetic data indicate a recent shortening rate of  $14 \pm 1 \text{ mm/yr}$  perpendicular to the strike of the orogen (Fig.32) (Banerjee 2002). For area A3 it is  $11.8 \pm 1$

mm/yr (Kundu et al. 2014). It is debated whether the oblique portion of the convergence is entirely accommodated via the Karakorum Fault Zone and maybe via the Kaurik-Chango Rift (Robinson 2009),(Lacassin et al. 2004),(Brown et al. 2002; Kundu et al. 2014). However the role of the Karakorum fault is not part of the discussion in this thesis but it is necessary to mention that the compressional regime in the Northwestern Himalaya is different than in the Central Himalaya.

Multiple studies performed in our three areas (A1-A3) showed that most of the perpendicular strain portion in the northwestern Himalaya is solely accommodated by thickening of its foreland fold- and thrust belt (Wesnousky & Kumar 1999),(Powers et al. 1998), (Vassallo et al. 2015), (Gavillot et al. 2016), (Thakur et al. 2014). These studies infer shortening rates from restorations of balanced cross-sections or from the incision into dated river terraces across fault zones. They provide very important information about the local accommodation of strain averaged over ten to hundred thousands of years. Comparing these data with our results, the distribution of the tectonic activity seems to be more diverse than we can infer from the 1D surveys. Our 2D approach reveals that the erosion rates in the hanging wall of the MBT and at the PT2 is not uniform. We observe significant changes in the steepness index implying steepening of landscapes by tectonic uplift. We relate this to a pronounced tectonic activity at fault segments faults in the recent past. These areas and segments are namely the regions around the PT2 north of the Kashmir basin, around the Kishtwar-Window, the Kullu-Rampur-Window and in the Garwhal region and the MBT segments, west of the Chenab outlet, at the Dhauladhar range.

But the most striking support for our assumptions is the oscillating pattern in the difference in the channel steepness between the hanging wall and the footwall along the MBT. If we assumed that the shortening of the Himalaya is mainly accommodated by the MFT and internal deformation of the Subhimalaya, we would expect a uniform distribution in the difference in channel steepness. However, we observe an increase in erosion for which the MBT is responsible in all three areas (A1-A3). Keeping in mind that the structural architecture in the subsurface is different in the areas A1-A3, it is even more surprising that we see this commonality.

### Relation to exhumation and denudation rates

Modelled mean exhumation rates inferred from AFT (Apatite Fission track ages) ages yield rates in the range of  $1.5 \pm 0.5$  mm/yr in vicinity of the southern flanks of the High Himalaya near the Beas and Sutlej and Garwhal region over the past 4 Ma (Thiede et al. 2009; Thiede & Ehlers 2013). Interestingly, these long term exhumation rates are in good agreement with estimates of basinwide erosion rates using  $^{10}\text{Be}$  terrestrial cosmogenic nuclide concentrations in Sutlej tributaries in the hangingwall of the PT2 in Sutlej and Garwhal region (area A1) (Olen et al., 2016). Based on the analysis of 12 catchments, Olen et al. measured an average denudation rate of  $0.75 \pm 0.8$  mm/yr. The highest rates fall in a range between 2 and 2.09 mm/yr. They explain the large scatter in these data, by the seasonality and the density in the vegetation (Olen et al. 2016). Due to the fact that the different methods act on slightly different time scales, it is very likely that the averaged denudation rates are comparable to the exhumation rates (Olen et al. 2016).

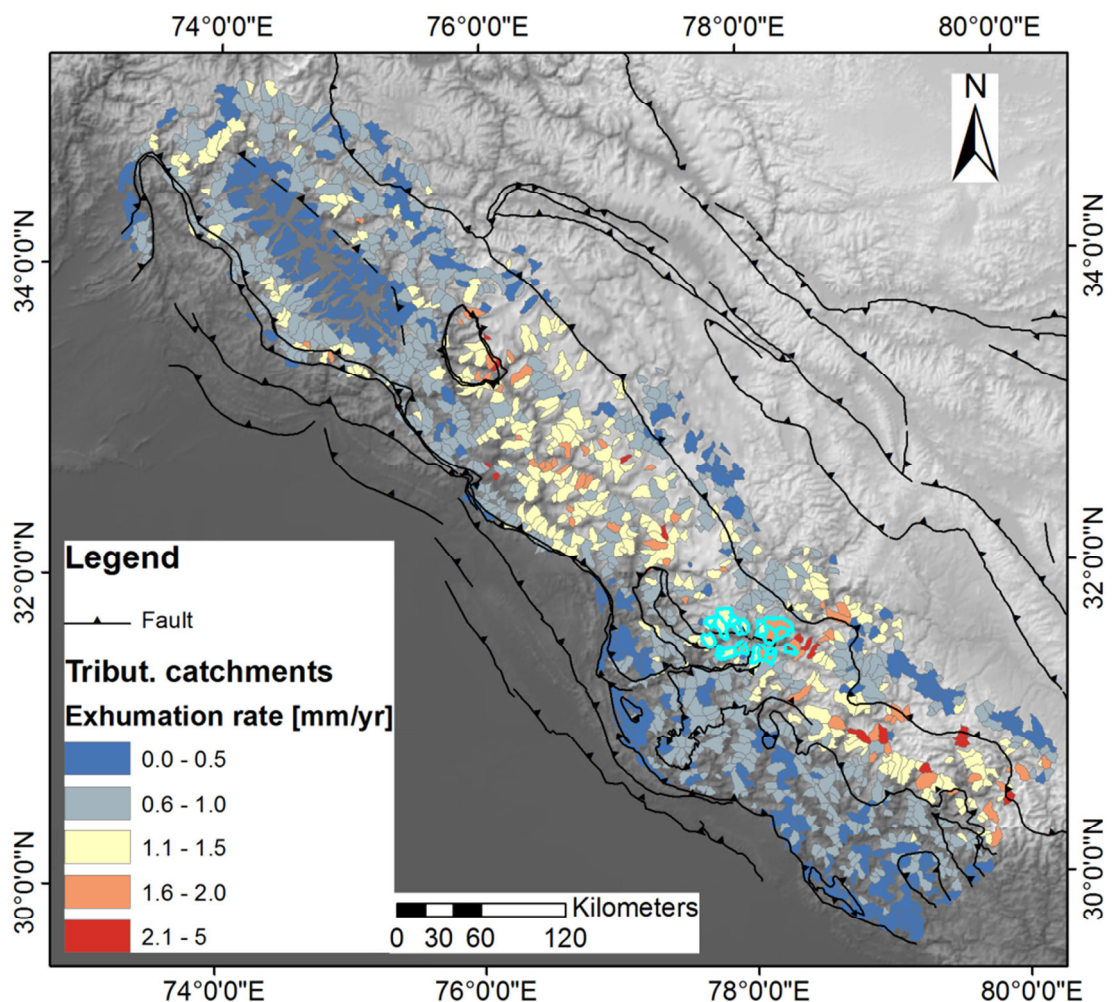


Figure 33. The correlation between normalized steepness indexes and modeled exhumation rates is based on AFT-ages of samples from the Kishtwar region (located in catchments with blue rim). The Subhimalaya is excluded because of the lithologic contrast between the crystalline rocks of the Lesser and Higher Himalaya and the weak sedimentites of the Subhimalaya.

The fact that short denudation rates and long-term exhumation rates fall in the same range possibly suggests that exhumation patterns are ongoing since several Myr and achieved or are close to a steady state setting. Moreover, it is very likely that the pronounced exhumation is regionally consistent during the Quaternary.

In order to test in how far our results can be correlated to these rates, we chose 20 catchments in the respective area along the transition between the Lesser and the Higher Himalayan (PT2) in and around the Kullu-Rampur window. The averaged steepness indexes of the drainage basins fall in a range between  $k_{sn} \sim 300$  and  $k_{sn} \sim 700$ . The scatter in the values is relatively low, therefore we assume that steepness indexes are better correlated with long-term exhumation rates. In order to obtain expected exhumation rates for every catchment in the Higher and Lower Himalaya in NW India we simply assume a linear dependency between the steepness index and modelled exhumation rate. The used scaling factor is 1/300. Thus, we assume that catchments draining crystalline lithologies with a  $k_{sn} > 300$  are exhuming with at least 1mm/yr. By using this correlation, we create an overview of the expected exhumation pattern in the Higher and Lower Himalaya of northwest India (Fig. 33). Reasonable results can be observed in the Lower Himalaya northeast of the Dehra Dun and the Nahan Salient (area A1). Here, we expect an exhumation rate below 1mm/yr. Assuming conditions close to a steady state, this rate also fits the published basin-wide erosion rates by Olen et al., 2016 (90% of the samples account for erosion rates between 0.2 and 1 mm/yr).

Furthermore we assume an exhumation rate at the Dhauladhar Range between 0.7 and 1.4 mm/yr and a rate between 1 and 2 mm/yr in the Lesser Himalayan units of the Kishtwar window. Both rates slightly underestimate the modeled rates obtained from AFT-ages (Thiede & Ehlers 2013). This either shows that the magnitude of the scaling factor or the linear correlation is not appropriate to use. Further deviations occur in recently glaciated areas. Some of the steep Chenab-tributaries north of the Dhauladhar Range suggest exhumation rates larger than 1.5 mm/yr. This does not correlate with modeled rates from AFT-ages which suggest a faster exhumation rate at the front of the Dhauladhar range than in its hinterland (Deeken et al. 2011). We assume that the local signal of these catchments has strongly been influenced by the last glacial maximum which had left deeply carved valleys (Eugster et al. 2016).

However, we know that this approach has to be developed and has to be shown to be reliable for the Himalaya. But the option to obtain expected rates is highly attractive because it includes the opportunity to make arguments about the exhumation of areas where no or just few data are available. Therefore it is worth trying to find included parameters and suitable

scaling factors in order to develop the understanding of exhumation or uplift and the resulting topography.

## Conclusion

We used normalized channel steepness indexes to determine the distribution of the erosion in the Northwestern Himalaya. The analysis of the river network revealed new insights, which have not been observed before in this context. We can draw 3 main conclusions from this thesis.

At first, the perpendicular profiles provide supporting facts for at least three different kinds of subsurface geometries which are necessary to describe the tectonic mechanisms in the northwestern Himalaya on a first order scale. The structural setting in area A1 is comparable to areas in the Central Himalaya. In area A2 we observe a different setting. The Lesser Himalaya is not well formed and the MBT probably contributes the main portion for the uplift of the Dhauladhar Range. In Area A3, the presence of the Kashmir Basin again requires another architecture of the subsurface, which is supported by the two peaks in the distribution of the steepness index orthogonal to the range front.

Second, the evaluation of our output with respect to the recent seismic activity and the GPS velocities in the region gives reasons to assume that, at least at some fault segments, out-of-sequence thrusting is apparent. The profile analysis revealed that out-of-sequence thrusting is necessary to maintain the immense presence of the PT2, forming the southern flanks of the High Himalaya. Otherwise, we cannot explain the significant number of steep catchments in the hangingwall of the respective structure and simultaneously observe the tremendous increase in elevation across the transition zone. That is why the tectonic uplift of the Greater Himalaya is necessary to explain our observation. In most of the places, we have no sufficient evidence for an in-sequence thrusting at that time.

However, the third point is that we assume changes in the erosion rate along strike of the PT2 but also along the MBT. For the PT2, respective areas are namely the regions north of the Kashmir basin, around the Kishtwar-Window, the Kullu-Rampur-Window and in the Garwhal region. For the MBT we expect that pronounced rock uplift is responsible for the increased denudation in the hangingwall of the fault segments, west of the Chenab outlet and at the Dhauladhar range.

## Reference

1. Ader, Thomas; Avouac, Jean-Philippe; Liu-Zeng, Jing; Lyon-Caen, Hélène; Bollinger, Laurent; Galetzka, John et al. (2012): *Convergence rate across the Nepal Himalaya and interseismic coupling on the Main Himalayan Thrust: Implications for seismic hazard.* In: *J. Geophys. Res.* 117 (B4), P. n/a. DOI: 10.1029/2011JB009071.
2. Arora, B. R.; Gahalaut, V. K.; Kumar, Naresh (2012): *Structural control on along-strike variation in the seismicity of the northwest Himalaya.* In: *Journal of Asian Earth Sciences* 57 (0), P. 15–24. DOI: 10.1016/j.jseaes.2012.06.001.
3. Avouac, J. P.; Cattin, R. (2000): *Modelling mountain building and the seismic cycle in the Himalaya of Nepal.* In: *J. Geophys. Res.* 105 (B6)
4. Banerjee, P. (2002): *Convergence across the northwest Himalaya from GPS measurements.* In: *Geophys. Res. Lett.* 29 (13). DOI: 10.1029/2002GL015184.
5. Banerjee, P.; Bürgmann, R.; Nagarajan, B.; Apel, E. (2008): *Intraplate deformation of the Indian subcontinent.* In: *Geophys. Res. Lett.* 35 (18). DOI: 10.1029/2008GL035468.
6. Bollinger, L.; Henry, P.; Avouac, J. P. (2006): *Mountain building in the Nepal Himalaya: Thermal and kinematic model.* In: *Earth and Planetary Science Letters* 244 (1-2), P. 58–71. DOI: 10.1016/j.epsl.2006.01.045.
7. Bookhagen, Bodo; Burbank, Douglas W. (2006): *Topography, relief, and TRMM-derived rainfall variations along the Himalaya.* In: *Geophys. Res. Lett.* 33 (8). DOI: 10.1029/2006GL026037.
8. Brocklehurst, Simon H.; Whipple, Kelin X. (2007): *Response of glacial landscapes to spatial variations in rock uplift rate.* In: *J. Geophys. Res.* 112 (F2). DOI: 10.1029/2006JF000667.
9. Brown, E. T.; Bendick, R.; Bourlès, D. L.; Gaur, V.; Molnar, P.; Raisbeck, G. M.; Yiou, F. (2002): *Slip rates of the Karakorum fault, Ladakh, India, determined using cosmic ray exposure dating of debris flows and moraines.* In: *J. Geophys. Res.* 107 (B9), P. ESE 7-1–ESE 7-13. DOI: 10.1029/2000JB000100.
10. Burbank, D. W.; Johnson, G. D. (1982): *Inter-montane basin development in the past 4 Myr in the north-west Himalaya.* In: *Nature* (298), P. 432–437.
11. Burbank, Douglas W. (1983): *The Chronology of intermontane-basin development in the northwestern Himalaya and the evolution of the Northwest Syntaxis.* In: *Earth and Planetary Science Letters* (64), P. 77–92.
12. Burbank, Douglas W.; Raynolds, Robert H.; Johnson, Gary D. (1986): *Late Cenozoic tectonics and sedimentation in the north-western Himalayan foredeep: II. Eastern limb*

- of the Northwest Synaxis and regional synthesis. In: Spec. Publs. in Ass. Sediment. (8), P. 293–306.*
13. Caldwell, Warren B.; Klemperer, Simon L.; Lawrence, Jesse F.; Rai, Shyam S.; Ashish (2013): Characterizing the Main Himalayan Thrust in the Garhwal Himalaya, India with receiver function CCP stacking. In: *Earth and Planetary Science Letters* 367, P. 15–27. DOI: 10.1016/j.epsl.2013.02.009.
  14. Chevalier, M-L; Ryerson, F. J.; Tapponnier, P.; Finkel, R. C.; Van Der Woerd, J; Haibing, Li; Qing, Liu (2005): Slip-rate measurements on the Karakorum Fault may imply secular variations in fault motion. In: *Science (New York, N.Y.)* 307 (5708), P. 411–414. DOI: 10.1126/science.1105466.
  15. Davis, D., Suppe,J. ,Dahlen F.A. (1983), Mechanics of fold-and-thrust belts and accretionary wedges, *J. Geophys. Res.*, 88(B2), 1153–1172, DOI:10.1029/JB088iB02p01153.
  16. Deeken, A.; Thiede, R. C.; Sobel, E. R.; Hourigan, J. K.; Strecker, M. R. (2011): Exhumational variability within the Himalaya of northwest India. In: *Earth and Planetary Science Letters* 305 (1-2), P. 103–114. DOI: 10.1016/j.epsl.2011.02.045.
  17. Elliott, J. R.; Jolivet, R.; Gonzalez, P. J.; Avouac, J.-P.; Hollingsworth, J.; Searle, M. P.; Stevens, V. L. (2016): Himalayan megathrust geometry and relation to topography revealed by the Gorkha earthquake. In: *Nature Geosci* 9 (2), P. 174–180
  18. England, Philip; Molnar, Peter (1990): Surface uplift, uplift of rocks, and exhumation of rocks. In: *Geol* 18 (12), P. 1173.
  19. England, Philip; Molnar, Peter (1997): The field of crustal velocity in Asia calculated from Quaternary rates of slip on faults. In: *J. Geophys. Res.* (130), P. 551–582.
  20. Eugster, Patricia; Scherler, Dirk; Thiede, Rasmus C.; Codilean, Alexandru T.; Strecker, Manfred R. (2016): Rapid Last Glacial Maximum deglaciation in the Indian Himalaya coeval with midlatitude glaciers: New insights from 10 Be-dating of ice-polished bedrock surfaces in the Chandra Valley, NW Himalaya. In: *Geophys. Res. Lett.* 43 (4), P. 1589–1597. DOI: 10.1002/2015GL066077.
  21. Gansser A. (Hg.) (1964): *Geology of the Himalayas*. Edited by L.U. de Sitter. London, New York, Sydney: Interscience Publisher by John Wiley and Sons Ltd. (Regional Geology Series).
  22. Gao, Rui; Lu, Zhanwu; Klemperer, Simon L.; Wang, Haiyan; Dong, Shuwen; Li, Wenhui; Li, Hongqiang (2016): Crustal-scale duplexing beneath the Yarlung Zangbo suture in the western Himalaya. In: *Nature Geosci* 9 (7), P. 555–560. DOI: 10.1038/NGEO2730.
  23. Gavillot, Y.; Meigs, A.; Yule, D.; Heermance, R.; Rittenour, T.; Madugo, C.; Malik, M. (2016): Shortening rate and Holocene surface rupture on the Riasi fault system in the Kashmir Himalaya: Active thrusting within the Northwest Himalayan orogenic wedge.

*In: Geological Society of America Bulletin 128 (7-8), P. 1070–1094. DOI: 10.1130/B31281.1.*

24. Hack, J. T. (1957): *Studies of Longitudinal Stream Profiles in Virginia and Maryland*. In: U.S. Geological Survey Professional Paper (294-B), P. 97
25. Hack, J. T. (1973): *Stream-profile analysis a stream-gradient index*. In: *Journal of research U.S. geol. survey* 1 (4), P. 421–429
26. Harvey, Jonathan E.; Burbank, Douglas W.; Bookhagen, Bodo (2015): *Along-strike changes in Himalayan thrust geometry: Topographic and tectonic discontinuities in western Nepal*. In: *Lithosphere* 7 (5), P. 511–518. DOI: 10.1130/L444.1.
27. Herman, Frédéric; Copeland, Peter; Avouac, Jean-Philippe; Bollinger, Laurent; Mahéo, Gweltaz; Le Fort, Patrick et al. (2010): *Exhumation, crustal deformation, and thermal structure of the Nepal Himalaya derived from the inversion of thermochronological and thermobarometric data and modeling of the topography*. In: *J. Geophys. Res.* 115 (B6). DOI: 10.1029/2008JB006126.
28. Hodges, K. V. (2000): *Tectonics of the Himalaya and southern Tibet from two perspectives*. In: *GSA Bulletin* (112), P. 324–350.
29. Hoffmann, T.; Müller, T.; Johnson, E. A.; Martin, Y. E. (2013): *Postglacial adjustment of steep, low-order drainage basins, Canadian Rocky Mountains*. In: *J. Geophys. Res. Earth Surf.* 118 (4), P. 2568–2584. DOI: 10.1002/2013JF002846.
30. Whipple, Kelin X.; Tucker, Gregory E.: *Dynamics of the stream-power river incision model: Implications for height limits of mountain ranges, landscape response timescales, and research needs*. In: *J. Geophys. Res. (Journal of Geophysical Research)* 104 (B8) P. 17661–17674
31. Kirby, Eric; Whipple, Kelin X. (2012): *Expression of active tectonics in erosional landscapes*. In: *Journal of Structural Geology* 44, P. 54–75. DOI: 10.1016/j.jsg.2012.07.009.
32. Kundu, Bhaskar; Yadav, Rajeev Kumar; Bali, Bikram Singh; Chowdhury, Sonalika; Gahalaut, V. K. (2014): *Oblique convergence and slip partitioning in the NW Himalaya: Implications from GPS measurements*. In: *Tectonics* 33 (10), P. 2013–2024. DOI: 10.1002/2014TC003633.
33. Seeber L., Gornitz V. (1983): *River Profiles along the Himalayan arc as indicators of active tectonics*. In: *Tectonophysics* (92), P. 335–367.
34. Lacassin, Robin; Valli, Franck; Arnaud, Nicolas; Leloup, P. Hervé; Paquette, Jean Louis; Haibing, Li et al. (2004): *Large-scale geometry, offset and kinematic evolution of the Karakorum fault, Tibet*. In: *Earth and Planetary Science Letters* 219 (3-4), P. 255–269. DOI: 10.1016/S0012-821X(04)00006-8.

35. Lavé, J.; Avouac, J. P. (2000): Active Folding of fluvial terraces across the Siwalik Hills. In: *J. Geophys. Res.* (105), P. 5735–5770.
36. Lavé, J.; Avouac, J. P. (2001): Fluvial incision and tectonic uplift across the Himalayas of central Nepal. In: *J. Geophys. Res.* 106 (B11), P. 26561–26591.
37. Meigs, Andrew J.; Burbank, Douglas W.; Beck, Richard A. (1995): Middle-late Miocene (>10 Ma) formation of the Main Boundary Thrust in the western Himalaya. In: *Geology* (23), P. 423–426.
38. Molnar, Peter; Stock, Joann M. (2009): Slowing of India's convergence with Eurasia since 20 Ma and its implications for Tibetan mantle dynamics. In: *Tectonics* 28 (3), P. n/a. DOI: 10.1029/2008TC002271.
39. Mugnier, Jean-Louis; Huyghe, Pascal (2006): Ganges basin geometry records a pre-15 Ma isostatic rebound of Himalaya. In: *Geology* 34 (6), P. 445–448.
40. Olen, Stephanie M.; Bookhagen, Bodo; Strecker, Manfred R. (2016): Role of climate and vegetation density in modulating denudation rates in the Himalaya. In: *Earth and Planetary Science Letters* 445, P. 57–67. DOI: 10.1016/j.epsl.2016.03.047.
41. Pandey, M. R.; Tandukar, R. P.; Avouac, J. P.; Lavé, J.; Massot, J. P. (1995): Interseismic Strain Accumulation on the Himalayan Crustal Ramp (Nepal). In: *Geophys. Res. Lett.* 22 (7), P. 751–754
42. Powers, Peter M.; Lillie, Robert J.; Yeats, Robert S. (1998): Structure and shortening of the Kangra and Dehra Dun reentrants, Sub-Himalaya, India. In: *Geological Society of America Bulletin* 110 (8), P. 1010–1027.
43. Robinson, Alexander C. (2009): Geologic offsets across the northern Karakorum fault: Implications for its role and terrane correlations in the western Himalayan-Tibetan orogen. In: *Earth and Planetary Science Letters* 279 (1-2), P. 123–130. DOI: 10.1016/j.epsl.2008.12.039.
44. Robinson, D. M.; DeCelles, P. G.; Garzione, C. N.; Pearson, O. N.; Harrison, T. M.; Catlos, E. J. (2003): Kinematic model for the Main Central thrust in Nepal. In: *Geology* 31 (4), P. 359–362.
45. Royden, Leigh; Taylor Perron, J. (2013): Solutions of the stream power equation and application to the evolution of river longitudinal profiles. In: *J. Geophys. Res. Earth Surf.* 118 (2), P. 497–518. DOI: 10.1002/jgrf.20031.
46. Schwanghart, W.; Scherler, D. (2014): Short Communication: TopoToolbox 2 – MATLAB-based software for topographic analysis and modeling in Earth surface sciences. In: *Earth Surf. Dynam.* 2 (1), P. 1–7. DOI: 10.5194/esurf-2-1-2014.

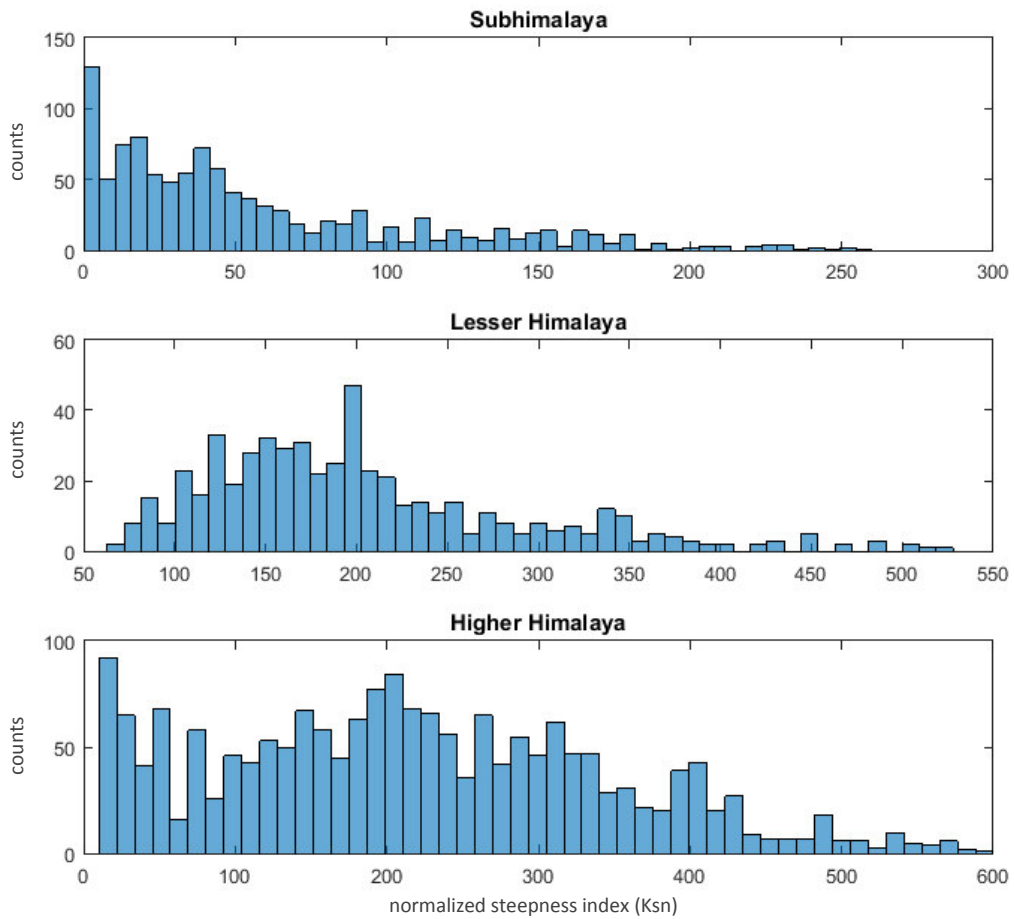
47. Schwanghart W., Kuhn N. J. (6): *TopoToolbox: A set of Matlab functions for topographic analysis*. In: *Environmental Modelling & Software* 2010, 6 (25), P. 770–781.
48. Silver, Calvin R. P.; Murphy, Michael A.; Taylor, Michael H.; Gosse, John; Baltz, Thomas (2015): *Neotectonics of the Western Nepal Fault System: Implications for Himalayan strain partitioning*. In: *Tectonics* 34 (12), P. 2494–2513. DOI: 10.1002/2014TC003730.
49. Singh, T.; Awasthi, A. K.; Caputo, R. (2012): *The sub-Himalayan fold-thrust belt in the 1905 Kangra earthquake zone: A critical taper model perspective for seismic hazard analysis*. In: *Tectonics* 31 (6), P. n/a. DOI: 10.1029/2012TC003120.
50. Stevens, V. L.; Avouac, J. P. (2015): *Interseismic coupling on the main Himalayan thrust*. In: *Geophys. Res. Lett.* 42 (14), P. 5828–5837. DOI: 10.1002/2015GL064845.
51. Strecker, M. R.; Frisch, W.; Hamburger, M. W.; Ratschbacher, L.; Semiletkin, S.; Zamoruyev, A.; Sturchio, N. (1995): *Quaternary deformation in the Eastern Pamirs, Tadzhikistan and Kyrgyzstan*. In: *Tectonics* 14 (5), P. 1061–1079. DOI: 10.1029/95TC00927.
52. Tapponnier, P.; Molnar, P. (1979): *Active faulting and Cenozoic tectonics of the Tien Shan, Mongolia, and Baykal regions*. In: *J. Geophys. Res.* 84, P. 3425–3459
53. Thakur, V. C. (1993): *Geology of Western Himalaya*. Oxford, New York: Pergamon Press (Physics and chemistry of the earth, v. 19).
54. Thakur, V. C.; Joshi, M.; Sahoo, D.; Suresh, N.; Jayangondapermal, R.; Singh, A. (2014): *Partitioning of convergence in Northwest Sub-Himalaya: estimation of late Quaternary uplift and convergence rates across the Kangra reentrant, North India*. In: *Int J Earth Sci (Geol Rundsch)* 103 (4), P. 1037–1056. DOI: 10.1007/s00531-014-1016-7.
55. Thakur, V. C.; Pandey, A. K.; Suresh, N. (2007): *Late Quaternary–Holocene evolution of Dun structure and the Himalayan Frontal Fault zone of the Garhwal Sub-Himalaya, NW India*. In: *Journal of Asian Earth Sciences* 29 (2-3), P. 305–319. DOI: 10.1016/j.jseaes.2006.02.002.
56. Thiede, Rasmus C.; Ehlers, Todd A.; Bookhagen, Bodo; Strecker, Manfred R. (2009): *Erosional variability along the northwest Himalaya*. In: *J. Geophys. Res.* 114 (F1). DOI: 10.1029/2008JF001010.
57. Thiede, R. C.; Ehlers, T. A. (2013): *Large spatial and temporal variations in Himalayan denudation*. In: *Earth and Planetary Science Letters* 371-372, P. 278–293. DOI: 10.1016/j.epsl.2013.03.004.
58. Vassallo, R.; Mugnier, J.-L.; Vignon, V.; Malik, M. A.; Jayangondaperumal, R.; Srivastava, P. et al. (2015): *Distribution of the Late-Quaternary deformation in*

*Northwestern Himalaya.* In: *Earth and Planetary Science Letters* 411, P. 241–252. DOI: 10.1016/j.epsl.2014.11.030.

59. Wang, Q.; Zhang, P. Z.; Freymueller, J. T.; Bilham, R.; Larson, K. M.; Lai, X. et al. (2001): *Present-day crustal deformation in China constrained by global positioning system measurements.* In: *Science (New York, N.Y.)* 294 (5542), P. 574–577. DOI: 10.1126/science.1063647.
60. Wesnousky, Steven G.; Kumar, Setnil (1999): *Uplift and Convergence along the Himalayan Frontal Thrust of India.* In: *Tectonics* (18), P. 967–976.
61. Whipple, Kelin X.; Shirzaei, Manoochehr; Hodges, Kip V.; Ramon Arrowsmith, J. (2016): *Active shortening within the Himalayan orogenic wedge implied by the 2015 Gorkha earthquake.* In: *Nature Geosci* 9 (9), P. 711–716. DOI: 10.1038/NGEO2797.
62. Whipple, Kelin X.; Tucker, Gregory E. (1999): *Dynamics of the stremppower river incision model: Implications for height limits of mountain ranges, landscape response timescales, and research needs.* In: *J. Geophys. Res.* 104 (B8), P. 17661–17674.
63. Whittaker, A. C. (2012): *How do landscapes record tectonics and climate?* In: *Lithosphere* 4 (2), P. 160–164. DOI: 10.1130/RF.L003.1.
64. Wobus, Cameron; Heimsath, Arjun; Whipple, Kelin; Hodges, Kip (2005): *Active out-of-sequence thrust faulting in the central Nepalese Himalaya.* In: *Nature* 434 (7036), P. 1008–1011. DOI: 10.1038/nature03499.
65. Wobus, Cameron; Whipple, Kelin X.; Kirby, Eric; Snyder, Noah; Johnson, Joel; Spyropoulos, Katerina et al. (2006a): *Tectonics from topography: Procedures, promise, and pitfalls.* In: *Special Paper 398: Tectonics, Climate, and Landscape Evolution, Bd. 398: Geological Society of America*, P. 55–74.
66. Wobus, Cameron W.; Whipple, Kelin X.; Hodges, Kip V. (2006b): *Neotectonics of the central Nepalese Himalaya: Constraints from geomorphology, detrital 40 Ar/ 39 Ar thermochronology, and thermal modeling.* In: *Tectonics* 25 (4), P. n/a. DOI: 10.1029/2005TC001935.
67. Wulf, Hendrik; Bookhagen, Bodo; Scherler, Dirk (2010): *Seasonal precipitation gradients and their impact on fluvial sediment flux in the Northwest Himalaya.* In: *Geomorphology* 118 (1-2), P. 13–21. DOI: 10.1016/j.geomorph.2009.12.003.

## Appendix

### Steepness Index Histograms



The histograms show the distribution of the catchment averaged steepness indexes in the different physiographic compartments. The maximum count column is below  $K_{sn} = 50$  in the Subhimalaya. In the Lesser Himalaya the peak is between  $K_{sn}=150$  and  $K_{sn}=200$ . For the High Himalaya we observe a peak value around  $K_{sn}=200$ . The cause for the different distributions is most likely the difference in the lithology. That is why we see low values in the weak substrate of the Subhimalaya which is more easily and faster to erode and high values in the more resistive units of the Lesser and the High Himalaya.

## Input Parameters

Matlab script: "Knickpoint Picker" by Alexander Neely and Bodo Bookhagen

```
area_threshold = 1e6;

min_drainage_area_to_process = 1e6;

min_dbasins_stats_to_process = 1e8;

stream_order = [3 4];

relief_values_m = [500 1000 1500];

str_areal = 1e6;

str_area2 = 1e7;

min_max_DA_fits = [1e6 1e10 100];

segL = 500;

min_str_gradient = 0.001;

MISC_FILES = 1;

REGEN = 1;

show_figs = 0

PaperType_size = 'A4';

min_trib_size = 100

smoothing_window = 201;

sgolayfilt_order = 11;

lumping_search_distance = 125;

min_kp_size1 = 1.5;

min_kp_size2 = 3;

min_kp_slope = 0.001;
```

**For further details and information according to the Matlab script, check:**

[Neely, A., Bookhagen, B., Burbank, D.W. \(in review\): Connecting Stream Transience and Hillslope Evolution: Insights from a Knickpoints Selection Algorithm applied to Santa Cruz Island, California, JGR-Earth Surface](#)